Journal of Computational Physics 475 (2023) 111869

Contents lists available at ScienceDirect

Journal of Computational Physics

journal homepage: www.elsevier.com/locate/jcp

High-order fully well-balanced numerical methods for one-dimensional blood flow with discontinuous properties

Ernesto Pimentel-García [a,*], Lucas O. Müller [b], Eleuterio F. Toro [c], Carlos Parés [a]

[a] Departamento de Análisis Matemático, Estadística e Investigación Operativa, y Matemática aplicada, Universidad de Málaga, Bulevar Louis Pasteur, 31, 29010, Málaga, Spain
[b] Department of Mathematics, University of Trento, Via Sommarive 14, 38123 Povo, Trento, Italy
[c] Laboratory of Applied Mathematics, University of Trento, Via Mesiano 77, 38123 Mesiano, Trento, Italy

ARTICLE INFO

Article history:
Received 11 June 2022
Received in revised form 18 November 2022
Accepted 18 December 2022
Available online 27 December 2022

Keywords:
Blood flows
Finite volume methods
Well-balanced methods
Reconstruction operators
Stationary solutions

ABSTRACT

In this paper, we are interested in the numerical study of the one-dimensional blood flow model with discontinuous mechanical and geometrical properties. We present the mathematical model together with its nondimensional form. We do an exhaustive investigation of all its stationary solutions and we propose high-order fully well-balanced numerical methods that are able to preserve all of them. They are based on the combination of the Generalized Hydrostatic Reconstruction and well-balanced reconstruction operators. These methods are able to deal with more than one discontinuous parameter. Several numerical tests are shown to prove its well-balanced and high-order properties, and its convergence to the exact solutions.

1. Introduction

One-dimensional blood flow models have been widely used in the past to address fundamental aspects of pulse wave propagation in the cardiovascular system [3,51,53], as well as to determine the state of certain conditions, as for example in [59,46,38]. Such models have also been used, in combination with lumped-parameter models, to construct comprehensive models of the cardiovascular system for the study of pathological states that act at a systemic level [39,50,9,45,60].

Mathematically, one-dimensional blood flow models are hyperbolic conservation laws, or at least systems of partial differential equations with hyperbolic-dominant behavior. Diffusive, dispersive and more complex terms might arise, especially when models include a richer-than-usual description of the blood-wall interaction by means of a so-called tube law [26]. In the most classical case blood flow is modeled with networks of one-dimensional hyperbolic systems of conservation (or balance) laws [12], where coupling conditions among vessels need to be specified [10,42], as well as inlet/outlet boundary conditions and the coupling to lumped-parameter models representing the peripheral vasculature [57]. In some applications, one-dimensional models are coupled to three-dimensional models, in order to provide realistic boundary conditions to such models [55,7,8].

In nature, vessels do not consist of perfectly cylindrical pipes, but present varying geometrical and mechanical properties. As a consequence, it is important that mathematical models for blood flow account for this variability. In terms of one-dimensional mathematical models, one has to consider tube laws that involve space-varying parameters. In turn, as the

* Corresponding author.
E-mail addresses: erpigar@uma.es (E. Pimentel-García), lucas.mueller@ing.unitn.it (L.O. Müller), eleuterio.toro@unitn.it (E.F. Toro), pares@uma.es (C. Parés).

https://doi.org/10.1016/j.jcp.2022.111869

reader will see in the next section, such variation implies that, for the system of equations written in conservative variables, i.e. cross-sectional vessel area and volumetric flow rate, the momentum balance equation includes source terms that depend on the spatial derivatives of tube law parameters [62]. These source terms are similar to those arising in other models, such as the shallow water equations with variable topography/channel width [4] or in the case of gas dynamics in pipes with variable duct cross-section [31]. These terms are often called *geometrical* source terms and pose particular challenges to the design of numerical schemes that are required to accurately approximate certain steady state solutions of the system under study (ideally with machine precision errors). Schemes that can preserve certain steady state solutions of the model are said to be *well-balanced*.

The literature on well-balanced schemes for blood flow is rather rich, with many methods proposed in the last decade. This variety regards the adopted methodologies and the type of solutions that methods preserve. Many researchers focused on techniques that consider the original 2×2 system [34], with a careful discretization of source terms arising from space-varying tube law parameters in order to preserve some or all the stationary solutions of the system: for instance, in [23] zero-velocity stationary solutions are preserved, in [27] low-Shapiro number stationary solutions, and in, [28,49,47] all of the stationary solutions. Methods that preserve zero-velocity stationary solutions are usually said to be well-balanced, while those preserving all the stationary solutions have been called exactly well-balanced, energy-balanced, or fully well-balanced: the latter will be used in this paper. Another possibility is to work in the context of discontinuous Galerkin schemes, for which some examples of well-balanced or fully well-balanced solvers are available [37,13]. Others in turn rely on a model reformulation, e.g. [62,58], that results in a non-conservative system and implies to work in the context of path-conservative numerical schemes [52]. Some applications of this technique for well-balanced solvers for friction-less one-dimensional blood flow are [44,58,43].

In [43] the need of fully well-balanced methods in order to capture correctly the right solutions of the problem was put on evidence. In that work, only one of the mechanical parameters of the model, the stiffness coefficient, was considered to be space-varying. The main goal of the present work is to develop high-order fully well-balanced numerical methods for the general case, in which all the mechanical and geometric parameters may be space-varying. The strategy described in [17] based on the design of well-balanced reconstruction operator will be followed. First-, second- and third-order semi-discrete high-order path-conservative schemes will be developed. A particular property of these methods is that for the case of constant parameters they reduce to conservative numerical methods for the original 2×2 blood flow model, avoiding concerns about the impact of integration path choices in the capacity of the numerical scheme to correctly describe shocks [1,15].

The rest of the paper is structured as follows. In section 2 we present the mathematical model and define steady state solutions of interest. Next, section 3 regards the design of second and third order accurate semi-discrete finite-volume type numerical schemes. Section 4 is devoted to the presentation of numerical results where we verify the implementation of the proposed numerical methods and assess their performance with respect to well-balanced properties, as well as regarding their capacity to correctly represent transient solutions. Finally, in section 5 we make final consideration on the presented work and results, as well as point out further developments.

2. Mathematical model

We consider the following formulation for one-dimensional blood flow in thin-walled deformable elastic tubes introduced in [62]:

$$\begin{cases} \partial_t A + \partial_x q = 0, \\ \partial_t q + \partial_x \left(\dfrac{q^2}{A} \right) + \dfrac{A}{\rho} \partial_x p = 0, \end{cases} \tag{2.1}$$

with

$$p(x,t) = K(x)\phi\left(\frac{A(x,t)}{A_0(x)}\right) + p_e(x),$$

where ϕ is the function defined by

$$\phi(a) = a^m - a^n. \tag{2.2}$$

The notation is as follows:

- $A(x,t)$ represents the cross-sectional area of the vessel.
- $q(x,t)$, the mass-flux and $u(x,t) = \dfrac{q(x,t)}{A(x,t)}$ is the averaged velocity of blood at a cross section.
- ρ, the fluid density, assumed to be constant.
- $A_0(x)$, the vessel cross-sectional area in an unloaded configuration.
- $K(x)$, the so-called stiffness coefficient, is a known positive function of the vessel wall Young modulus $E(x)$, the wall thickness $h_0(x)$ and $A_0(x)$.

- $p(x,t)$, the internal pressure.
- $p_e(x)$, the external pressure acting on the vessel.
- Here we assume $m > 0$ and $n \in (-2, 0]$. Typical values for collapsible tubes, such as veins, are $m = 10$, $n = -3/2$. For arteries we have $m = 1/2$, $n = 0$. Moreover, the specified intervals for m and n guarantee the genuine nonlinearity of certain characteristic fields [62], as explained later.

Let us now introduce the functions:

$$\Phi(a) = \int_0^a \phi(\tau)\, d\tau = \left(\frac{1}{m+1} a^{m+1} - \frac{1}{n+1} a^{n+1} \right), \tag{2.3}$$

$$\tilde{\Phi}(a) = \int_0^a \tau \phi'(\tau)\, d\tau = \left(\frac{m}{m+1} a^{m+1} - \frac{n}{n+1} a^{n+1} \right) \tag{2.4}$$

and note that the following equality holds:

$$\Phi(a) + \tilde{\Phi}(a) = a\phi(a). \tag{2.5}$$

Moreover, we note that the momentum equation can be rewritten as follows:

$$\partial_t q + \partial_x \left(\frac{q^2}{A} \right) + a \frac{K}{\rho} \partial_a \phi\, \partial_x A - a^2 \frac{K}{\rho} \partial_a \phi\, \partial_x A_0 + \frac{A}{\rho} \phi \partial_x K + \frac{A}{\rho} \partial_x p_e = 0, \tag{2.6}$$

where

$$a = \frac{A}{A_0}, \quad \phi = \phi(a), \quad \partial_a \phi = \frac{d\phi}{da}(a).$$

If we define now

$$\boldsymbol{U} = \begin{pmatrix} A \\ q \end{pmatrix}, \quad \boldsymbol{W} = \begin{pmatrix} A \\ q \\ K \\ A_0 \\ p_e \end{pmatrix}, \quad \boldsymbol{F}(\boldsymbol{W}) = \begin{pmatrix} q \\ \dfrac{q^2}{A} + \dfrac{K A_0}{\rho} \tilde{\Phi}\left(\dfrac{A}{A_0} \right) \end{pmatrix}, \tag{2.7}$$

it can be easily checked that the second component of $\partial_x F(\boldsymbol{W})$ is equal to:

$$\partial_x \left(\frac{q^2}{A} \right) + a \frac{K}{\rho} \partial_a \phi \partial_x A - a^2 \frac{K}{\rho} \partial_a \phi \partial_x A_0 + \frac{A_0}{\rho} \tilde{\Phi}(a) \partial_x K + \frac{K}{\rho} \tilde{\Phi}(a) \partial_x A_0.$$

If this expression is compared to (2.6) and (2.5) is used, one has that system (2.1) can be written in the form of a system of balance laws as follows:

$$\partial_t \boldsymbol{U} + \partial_x \boldsymbol{F}(\boldsymbol{W}) + \boldsymbol{S}_1(\boldsymbol{W}) \partial_x K + \boldsymbol{S}_2(\boldsymbol{W}) \partial_x A_0 + \boldsymbol{S}_3(\boldsymbol{W}) \partial_x p_e = 0, \tag{2.8}$$

where:

$$\boldsymbol{S}_1(\boldsymbol{W}) = \begin{pmatrix} 0 \\ \dfrac{A_0}{\rho} \Phi(a) \end{pmatrix}, \quad \boldsymbol{S}_2(\boldsymbol{W}) = -\begin{pmatrix} 0 \\ \dfrac{K}{\rho} \tilde{\Phi}(a) \end{pmatrix}, \quad \boldsymbol{S}_3(\boldsymbol{W}) = \begin{pmatrix} 0 \\ \dfrac{A}{\rho} \end{pmatrix}. \tag{2.9}$$

The vector notation:

$$\boldsymbol{S}(\boldsymbol{W}) = (\boldsymbol{S}_1(\boldsymbol{W}) \mid \boldsymbol{S}_2(\boldsymbol{W}) \mid \boldsymbol{S}_3(\boldsymbol{W})), \quad \boldsymbol{\sigma} = \begin{pmatrix} K \\ A_0 \\ p_e \end{pmatrix}, \tag{2.10}$$

allows us to write system (2.8) in compact form as follows:

$$\partial_t \boldsymbol{U} + \partial_x \boldsymbol{F}(\boldsymbol{W}) + \boldsymbol{S}(\boldsymbol{W}) \cdot \partial_x \boldsymbol{\sigma} = 0. \tag{2.11}$$

The system can also be written in quasi-linear form:

$$\partial_t \boldsymbol{W} + \boldsymbol{\mathcal{A}}(\boldsymbol{W}) \partial_x \boldsymbol{W} = 0, \tag{2.12}$$

with:

$$\boldsymbol{\mathcal{A}}(\boldsymbol{W}) = \begin{pmatrix} 0 & 1 & 0 & 0 & 0 \\ -u^2 + a\frac{K}{\rho}\partial_a\phi & 2u & \frac{A}{\rho}\phi & -a^2\frac{K}{\rho}\partial_a\phi & \frac{A}{\rho} \\ 0 & 0 & 0 & 0 & 0 \\ 0 & 0 & 0 & 0 & 0 \\ 0 & 0 & 0 & 0 & 0 \end{pmatrix}, \tag{2.13}$$

The eigenvalues of $\boldsymbol{\mathcal{A}}(\boldsymbol{W})$ are:

$$\lambda_1 = u - c, \quad \lambda_2 = \lambda_3 = \lambda_4 = 0, \quad \lambda_5 = u + c,$$

with

$$c = \sqrt{a\frac{K}{\rho}\partial_a\phi}.$$

For parameter ranges previously introduced, system (2.12) is hyperbolic [62], since the matrix is diagonalizable, but not strictly hyperbolic.

The flow regime is characterized by the Shapiro number

$$S_h = \frac{|u|}{c}.$$

The flow corresponding to a state $[A, q, K, A_0, p_e]^T$ is said to be subcritical (or subsonic) if $S_h < 1$, critical (or sonic) if $S_h = 1$ and supercritical (or supersonic) if $S_h > 1$.

2.1. Weak solutions

Since the source term involves a nonconservative product, the definition of weak solutions is ambiguous and the theory of DalMasso, LeFloch and Murat [22] is followed. A family of paths:

$$\boldsymbol{\Psi}(s; \boldsymbol{W}_l, \boldsymbol{W}_r) = \begin{bmatrix} \boldsymbol{\Psi}_{\boldsymbol{U}}(s; \boldsymbol{W}_l, \boldsymbol{W}_r) \\ \boldsymbol{\Psi}_{\boldsymbol{\sigma}}(s; \boldsymbol{W}_l, \boldsymbol{W}_r) \end{bmatrix} = \begin{bmatrix} \Psi_A(s; \boldsymbol{W}_l, \boldsymbol{W}_r) \\ \Psi_q(s; \boldsymbol{W}_l, \boldsymbol{W}_r) \\ \Psi_K(s; \boldsymbol{W}_l, \boldsymbol{W}_r) \\ \Psi_{A_0}(s; \boldsymbol{W}_l, \boldsymbol{W}_r) \\ \Psi_{p_e}(s; \boldsymbol{W}_l, \boldsymbol{W}_r) \end{bmatrix}, \quad s \in [0, 1]$$

is selected that determines the Rankine-Hugoniot (RH) condition at the jumps:

$$\lambda[\boldsymbol{W}] = \int_0^1 \boldsymbol{\mathcal{A}}(\boldsymbol{\Psi}(s; W_l, W_r)) \frac{\partial}{\partial s}\boldsymbol{\Psi}(s; \boldsymbol{W}_l, \boldsymbol{W}_r)\, ds, \tag{2.14}$$

where λ is the shock speed, $[\boldsymbol{W}] = \boldsymbol{W}_r - \boldsymbol{W}_l$ and $\boldsymbol{W}_l, \boldsymbol{W}_r$, the left and right states respectively.

For any family of paths such that:

$$\boldsymbol{\sigma}_l = \boldsymbol{\sigma}_r = \boldsymbol{\sigma} \implies \boldsymbol{\Psi}_{\boldsymbol{\sigma}}(s; \boldsymbol{W}_l, \boldsymbol{W}_r) = \boldsymbol{\sigma}, \quad \forall s \in [0, 1], \tag{2.15}$$

the RH condition reduces to the standard one:

$$\lambda[\boldsymbol{U}] = \boldsymbol{F}(\boldsymbol{U}_r, \boldsymbol{\sigma}) - \boldsymbol{F}(\boldsymbol{U}_l, \boldsymbol{\sigma}), \tag{2.16}$$

in regions where $\boldsymbol{\sigma}$ is continuous. In effect, if $\boldsymbol{\sigma}_l = \boldsymbol{\sigma}_r = \boldsymbol{\sigma}$ one has

$$\lambda[\boldsymbol{W}] = \lambda \begin{bmatrix} [\boldsymbol{U}] \\ 0 \end{bmatrix}$$

and, on the other hand,

$$\int_0^1 \boldsymbol{\mathcal{A}}(\boldsymbol{\Psi})\partial_s\boldsymbol{\Psi}\, ds = \begin{bmatrix} \int_0^1 \left(\boldsymbol{J}(\boldsymbol{\Psi})\partial_s\boldsymbol{\Psi}_{\boldsymbol{U}} + \boldsymbol{S}(\boldsymbol{\Psi})\partial_s\boldsymbol{\Psi}_{\boldsymbol{\sigma}}\right) ds \\ 0 \end{bmatrix} = \begin{bmatrix} [\boldsymbol{F}(\boldsymbol{U}_r, \boldsymbol{\sigma}) - \boldsymbol{F}(\boldsymbol{U}_l, \boldsymbol{\sigma}) \\ 0 \end{bmatrix},$$

where $\boldsymbol{J}(\boldsymbol{W})$ represents the Jacobian of $\boldsymbol{F}$ (which is a 5×2 matrix) and the dependence on $(s; \boldsymbol{W}_l, \boldsymbol{W}_r)$ has been dropped for shortness. Observe that $\partial_s \boldsymbol{\Psi}_{\boldsymbol{\sigma}} \equiv 0$ because of (2.15). Therefore, (2.14) is equivalent to (2.16) in this case.

If $\boldsymbol{\sigma}_l \neq \boldsymbol{\sigma}_r$ the three final equations in the RH conditions:

$$\lambda(K_r - K_l) = 0, \quad \lambda(A_{0,r} - A_{0,l}) = 0, \quad \lambda(p_{e,r} - p_{e,l}) = 0,$$

imply that $\lambda = 0$ and the RH reduces to:

$$\boldsymbol{F}(\boldsymbol{U}_r, \boldsymbol{\sigma}_r) - \boldsymbol{F}(\boldsymbol{U}_l, \boldsymbol{\sigma}_l) + \int_0^1 \boldsymbol{S}(\boldsymbol{\Psi}(s)) \cdot \frac{\partial \boldsymbol{\Psi}_{\boldsymbol{\sigma}}}{\partial s}(s)\, ds = 0, \tag{2.17}$$

where $\boldsymbol{\Psi}(s) = \boldsymbol{\Psi}(s; \boldsymbol{W}_l, \boldsymbol{W}_r)$. Therefore, the selection of the family of paths only affects the jump condition satisfied at stationary contact discontinuities standing on a jump of the vector-valued function $\boldsymbol{\sigma}$. In order to select the family of paths in a natural way, let us study the Riemann invariants of the null eigenvalue. It can be easily checked that, given $\boldsymbol{W}$, the eigenspace of the null eigenvalue of $\boldsymbol{\mathcal{A}}(\boldsymbol{W})$, i.e. the set of vectors $\boldsymbol{Y} = [y_1, \ldots, y_5]^T \in \mathbb{R}^5$ such that

$$\mathcal{A}(\boldsymbol{W})\boldsymbol{Y} = 0,$$

is composed by the vectors $\boldsymbol{Y}$ satisfying:

$$y_2 = 0, \quad \left(-u^2 + a\frac{K}{\rho}\partial_a\phi\right) y_1 + \frac{A}{\rho}\phi y_3 - a^2\frac{K}{\rho}\partial_a\phi y_4 + \frac{A}{\rho} y_5 = 0.$$

One has then that any curve in the space of states $s \to \boldsymbol{W}(s) = [A(s), q(s), K(s), A_0(s), p_e(s)]^T$ satisfying:

$$q(s) = constant, \quad \frac{\rho}{2}\frac{q(s)^2}{A(s)^2} + K(s)\phi\left(\frac{A(s)}{A_0(s)}\right) + p_e(s) = constant$$

is an integral curve of the null eigenvalue, i.e. it satisfies

$$\mathcal{A}(\boldsymbol{W}(s))\partial_s \boldsymbol{W}(s) = 0, \quad \forall s,$$

as it can be easily verified by differentiating the above expression with respect to s. In this sense, the Riemann invariants associated to the null eigenvalue are:

$$q, \quad \frac{\rho}{2}\frac{q^2}{A^2} + K\phi\left(\frac{A}{A_0}\right) + p_e.$$

Therefore, it is natural to assume that a pair of states $(\boldsymbol{W}_l, \boldsymbol{W}_r)$ can be linked by an admissible contact discontinuity standing on a jump of K, A_0 or p_e if:

$$q_l = q_r, \quad \frac{\rho}{2}u_l^2 + K_l\phi\left(\frac{A_l}{A_{0,l}}\right) + p_{e,l} = \frac{\rho}{2}u_r^2 + K_r\phi\left(\frac{A_r}{A_{0,r}}\right) + p_{e,r}. \tag{2.18}$$

If the family of paths is such that the path $\boldsymbol{\Psi}(s; \boldsymbol{W}_l, \boldsymbol{W}_r)$ linking a pair of states satisfying (2.18) is a parameterization of the arc of the curve:

$$q = q_l, \quad \frac{\rho}{2}u^2 + K\phi(A) = \frac{\rho}{2}u_l^2 + K_l\phi(A_l),$$

that connect both states, then it can be easily shown that (2.17) is automatically satisfied.

2.2. Nondimensional form

Here we describe the nondimensionalization of system (2.1). Due to the need of dealing with very small values for some variables, it becomes necessary to work with the equations written in this form in order to avoid oscillations when we increase the order of accuracy of the numerical methods.

If the following nondimensional variables are chosen:

$$x' = \frac{x}{\overline{L}}, \quad t' = \frac{t}{\overline{T}}, \quad A' = \frac{A}{\overline{A}}, \quad q' = \frac{q}{\overline{A}\,\overline{U}}, \quad p' = \frac{p}{\rho\overline{U}^2},$$

where $\overline{L}$, $\overline{T}$, $\overline{A}$ are the characteristic length, time, cross-sectional area, and $\overline{U} = \overline{L}/\overline{T}$, then system (2.1) can be written as:

$$\begin{cases} \partial_{t'} A' + \partial_{x'} q' = 0, \\ \partial_{t'} q' + \partial_{x'} \left(\dfrac{(q')^2}{A'} \right) + A' \partial_{x'} p' = 0, \end{cases} \tag{2.19}$$

with:

$$p' = \overline{S}_h^{-2} K' \phi \left(\frac{A'}{A'_0} \right) + \overline{S}_{h,e}^{-2} p'_e$$

and:

$$\overline{S}_h = \frac{\overline{U}}{\sqrt{\overline{K}/\rho}}, \quad \overline{S}_{h,e} = \frac{\overline{U}}{\sqrt{\overline{p_e}/\rho}},$$

are dimensionless numbers, and $\overline{K}$, $\overline{p_e}$ represent the characteristic values of K and p_e and $K' = K/\overline{K}$, $p'_e = p_e/\overline{p_e}$, $A'_0 = A_0/\overline{A}$.

It can be easily checked that system (2.19) can be written in the form (2.11) with the states, fluxes, and sources given again by (2.7), (2.9) just by changing the variables by their non-dimensional counterparts, ρ by $\overline{S}_h^2$ in $\boldsymbol{F}(\boldsymbol{U})$, $\boldsymbol{S}_i(\boldsymbol{U})$, $i = 1, 2$, and ρ by $\overline{S}_{h,e}^2$ in $\boldsymbol{S}_3(\boldsymbol{U})$.

2.3. Stationary solutions

Since stationary solutions $\boldsymbol{U}^* = [A^*, q^*]^T$ can be interpreted as parametrization with x of integral curves of the null eigenvalue, they are implicitly given by:

$$q^* = C, \quad \frac{\rho}{2} \frac{(q^*)^2}{A^*(x)^2} + K(x) \phi \left(\frac{A^*(x)}{A_0(x)} \right) + p_e(x) = \Gamma, \tag{2.20}$$

where C and Γ are given constants. Given a point x, $A^*(x)$ has to satisfy the equation in the A variable:

$$f(A; C, \Gamma, K(x), A_0(x), p_e(x)) = 0,$$

where:

$$f(A; C, \Gamma, K, A_0, p_e) = \frac{\rho}{2} \frac{C^2}{A^2} + K \phi \left(\frac{A}{A_0} \right) + p_e - \Gamma, \tag{2.21}$$

whose first and second derivative with respect to A are given by:

$$f'(A; C, \Gamma, K, A_0, p_e) \equiv f'(A) = -\rho \frac{C^2}{A^3} + \frac{K}{A_0} \left[m \left(\frac{A}{A_0} \right)^{m-1} - n \left(\frac{A}{A_0} \right)^{n-1} \right], \tag{2.22}$$

$$f''(A; C, \Gamma, K, A_0, p_e) \equiv f''(A) = 3\rho \frac{C^2}{A^4} + \frac{K}{A_0^2} \left[m(m-1) \left(\frac{A}{A_0} \right)^{m-2} - n(n-1) \left(\frac{A}{A_0} \right)^{n-2} \right]. \tag{2.23}$$

We now proceed by describing noteworthy properties of function (2.21).

2.3.1. Blood-at-rest case

If $C = 0$, the function reduces to

$$f(A) = K \left[\left(\frac{A}{A_0} \right)^m - \left(\frac{A}{A_0} \right)^n \right] + p_e - \Gamma,$$

then

1. If $n = 0$:
   - $f(0) = -K + p_e - \Gamma$.
   - $\lim_{A \longrightarrow +\infty} f(A) = +\infty$.
   - $f'(A) = Km \dfrac{A^{m-1}}{A_0^m} > 0, \forall A > 0$.

   Then f is strictly increasing: it has a root if and only if $p_e \leq (\Gamma + K)$ and it is unique.
2. If $n \in (-2, 0)$:
   - $\lim_{A \longrightarrow 0^+} f(A) = -\infty$.
   - $\lim_{A \longrightarrow +\infty} f(A) = +\infty$.

- $f'(A) = \frac{K}{A_0}\left[m\left(\frac{A}{A_0}\right)^{m-1} - n\left(\frac{A}{A_0}\right)^{n-1}\right] > 0, \forall A > 0.$

Then f is again strictly increasing and it has always a unique root in $(0, +\infty)$.

2.3.2. General case

If $C \neq 0$, one has:

- $\lim_{A \longrightarrow 0^+} f(A) = +\infty.$
- $\lim_{A \longrightarrow +\infty} f(A) = +\infty.$
- $f'(A) = 0 \iff \frac{K}{A_0}\left[m\left(\frac{A}{A_0}\right)^{m-1} - n\left(\frac{A}{A_0}\right)^{n-1}\right] = \rho\frac{C^2}{A^3} \iff K\left[m\frac{A^{m+2}}{A_0^m} - n\frac{A^{n+2}}{A_0^n}\right] = \rho C^2.$

The function

$$g(A; K, C) \equiv g(A) = K\left[m\frac{A^{m+2}}{A_0^m} - n\frac{A^{n+2}}{A_0^n}\right] - \rho C^2 \tag{2.24}$$

satisfies:

– $\lim_{A \longrightarrow 0^+} g(A) = -\rho C^2 < 0.$

– $\lim_{A \longrightarrow +\infty} g(A) = +\infty.$

– $g'(A) = K\left[m(m+2)\frac{A^{m+1}}{A_0^m} - n(n+2)\frac{A^{n+1}}{A_0^n}\right] > 0, \quad \forall A > 0.$

Therefore g has a unique root, A_{crit}, that corresponds to a minimum of f. It can be checked that the state defined by $A = A_{crit}$, $q = C$ is critical.

We can conclude the following:

- If $f(A_{crit}) < 0$, then f has two roots: it can be shown that one of them, A_{sub}, corresponds to a subcritical regime and the other one, A_{sup}, to a supercritical one: see [43] for details.
- If $f(A_{crit}) = 0$, then A_{crit} is the only root of f and it is critical.
- If $f(A_{crit}) > 0$, then f has not roots.

3. High-order fully well-balanced numerical methods

For simplicity, we consider here uniform meshes composed by cells $I_i = [x_{i-1/2}, x_{i+1/2}]$ of length Δx whose midpoints are represented by x_i. The mesh is assumed to be designed so that the discontinuity points of function K, A_0 or p_e are placed at the interface between two computational cells.

Following [52], we consider semi-discrete finite-volume methods of the form:

$$\frac{d\boldsymbol{W}_i}{dt} = -\frac{1}{\Delta x}\left(\mathbb{D}^-_{i+\frac{1}{2}} + \mathbb{D}^+_{i-\frac{1}{2}} + \int_{x_{i-\frac{1}{2}}}^{x_{i+\frac{1}{2}}} \boldsymbol{\mathcal{A}}(\mathbb{P}_i^t(x))\frac{\partial}{\partial x}\mathbb{P}_i^t(x)dx\right), \tag{3.1}$$

where:

- $\boldsymbol{W}_i(t) \cong \frac{1}{\Delta x}\int_{x_{i+\frac{1}{2}}}^{x_{i-\frac{1}{2}}} \boldsymbol{W}(x,t)\,dx$ is the approximation to the cell average of the solution at the i-th cell at time t;
- $\mathbb{P}_i^t(x) = \mathbb{P}_i(x; \{\boldsymbol{W}_j(t)\}_{j\in\mathcal{S}_i})$ is a high-order well-balanced operator in the sense defined in [17], i.e. an operator that gives a smooth high-order approximation of the solution at the i-th cell from the values of the cell average approximations available at cells belonging to the stencil $\mathcal{S}_i$;
- $\mathbb{D}^{\pm}_{i+\frac{1}{2}} = \mathbb{D}^{\pm}\left(\boldsymbol{W}^-_{i+\frac{1}{2}}, \boldsymbol{W}^+_{i+\frac{1}{2}}\right)$, where:

$$\boldsymbol{W}^-_{i+\frac{1}{2}}(t) = \mathbb{P}_i^t(x_{i+\frac{1}{2}}), \quad \boldsymbol{W}^+_{i+\frac{1}{2}}(t) = \mathbb{P}_{i+1}^t(x_{i+\frac{1}{2}})$$

are the reconstructions at the cell interface and $\mathbb{D}^{\pm}(\boldsymbol{W}_l, \boldsymbol{W}_r)$ are the fluctuations corresponding to a first-order path-conservative numerical method

$$\boldsymbol{W}_i^{n+1} = \boldsymbol{W}_i^n - \frac{\Delta t}{\Delta x}\left(\mathbb{D}^+(\boldsymbol{W}_{i-1}^n, \boldsymbol{W}_i^n) + \mathbb{D}^-(\boldsymbol{W}_i^n, \boldsymbol{W}_{i+1}^n)\right), \tag{3.2}$$

for which:

$$\mathbb{D}^{\pm}(\boldsymbol{W},\boldsymbol{W})=0,\quad \forall \boldsymbol{W} \tag{3.3}$$

and:

$$\mathbb{D}^{-}(\boldsymbol{W}_l,\boldsymbol{W}_r)+\mathbb{D}^{+}(\boldsymbol{W}_l,\boldsymbol{W}_r)=\int_0^1 \boldsymbol{\mathcal{A}}(\boldsymbol{\Psi}(s))\frac{\partial \boldsymbol{\Psi}}{\partial s}(s)\,ds \tag{3.4}$$

$$=\begin{bmatrix} \boldsymbol{F}(\boldsymbol{U}_r,\boldsymbol{\sigma}_r)-\boldsymbol{F}(\boldsymbol{U}_l,\boldsymbol{\sigma}_l)+\int_0^1 \boldsymbol{S}(\boldsymbol{\Psi}(s))\cdot\frac{\partial \boldsymbol{\Psi}_{\boldsymbol{\sigma}}}{\partial s}(s)\,ds \\ 0 \end{bmatrix},\quad \forall \boldsymbol{W}_l,\boldsymbol{W}_r,$$

where $\boldsymbol{\Psi}(s)=\boldsymbol{\Psi}(s;\boldsymbol{W}_l,\boldsymbol{W}_r)$, $s\in[0,1]$ is a family of paths joining $\boldsymbol{W}_l$ with $\boldsymbol{W}_r$.

Definition 1. The numerical method (3.1) is said to be fully well-balanced if the sequence of cell averages $\{\boldsymbol{W}_i^*\}$ of any stationary solution $\boldsymbol{W}^*$ verifying (2.20) is an equilibrium of the ODE (3.1).

It can be easily checked that (3.1) is fully well-balanced if both the first-order path-conservative method used for computing $\mathbb{D}^{\pm}$ and the reconstruction operator are fully well-balanced according to the following definitions.

Definition 2. The first-order path-conservative numerical method (3.2) whose fluctuations are $\mathbb{D}^{\pm}$ is said to be fully well-balanced if

$$\mathbb{D}^{\pm}(\boldsymbol{W}_l,\boldsymbol{W}_r)=0$$

for $\boldsymbol{W}_l$ and $\boldsymbol{W}_r$ such that

$$q_l=q_r,\quad \Gamma(\boldsymbol{W}_l)=\Gamma(\boldsymbol{W}_r), \tag{3.5}$$

where

$$\Gamma(\boldsymbol{W})=\frac{\rho}{2}\frac{q}{A^2}+K\phi\left(\frac{A}{A_0}\right)+p_e. \tag{3.6}$$

Definition 3. The reconstruction operator $\{\mathbb{P}_i(x)\}$ is said to be fully well-balanced if, when it is applied to the sequence of cell averages $\{\boldsymbol{W}_i^*\}$ of any stationary solution $\boldsymbol{W}^*$ verifying (2.20), one has

$$\mathbb{P}_i(x)=\boldsymbol{W}^*(x),\quad \forall x\in[x_{i-1/2},x_{i+1/2}],\quad \forall i,$$
$$\boldsymbol{W}^{\pm}_{i+\frac{1}{2}}=\boldsymbol{W}^*(x^{\pm}_{i+1/2}).$$

3.1. First-order fully well-balanced path-conservative method

We consider the Generalized Hydrostatic Reconstruction (GHR) technique introduced in [16] as a generalization of the hydrostatic reconstruction technique introduced in [2] (which was further enhanced in [6]) to obtain schemes that preserve the solutions corresponding to water at rest for the shallow water equations. It is based on a family of paths constructed as follows. Given two arbitrary states:

$$\boldsymbol{W}_l=\begin{bmatrix}\boldsymbol{U}_l\\ \boldsymbol{\sigma}_l\end{bmatrix},\quad \boldsymbol{W}_r=\begin{bmatrix}\boldsymbol{U}_r\\ \boldsymbol{\sigma}_r\end{bmatrix},$$

we proceed as follows:

- First a vector of intermediate values:

$$\boldsymbol{\sigma}_0=\begin{pmatrix}K_0\\ A_{0,0}\\ p_{e,0}\end{pmatrix}$$

between $\boldsymbol{\sigma}_l$ and $\boldsymbol{\sigma}_r$ is selected such that $\boldsymbol{\sigma}_0=\boldsymbol{\sigma}_l=\boldsymbol{\sigma}_r$ whenever $\boldsymbol{\sigma}_l=\boldsymbol{\sigma}_r$. The particular choice of intermediate states using here will be detailed in Subsection 3.2.

- Then, then the following intermediate states are considered:
  - The states $\boldsymbol{W}_0^{-,1} = [A^{-,1}, q_l, K_l, A_{0,l}, p_{e,0}]^T$, $\boldsymbol{W}_0^{+,1} = [A^{+,1}, q_r, K_r, A_{0,r}, p_{e,0}]^T$ where $A^{\pm,1}$ satisfy:

$$\frac{\rho}{2}\frac{q_l^2}{(A^{-,1})^2} + K_l\phi\left(\frac{A^{-,1}}{A_{0,l}}\right) + p_{e,0} = \Gamma(\boldsymbol{W}_l), \tag{3.7}$$

$$\frac{\rho}{2}\frac{q_r^2}{(A^{+,1})^2} + K_r\phi\left(\frac{A^{+,1}}{A_{0,r}}\right) + p_{e,0} = \Gamma(\boldsymbol{W}_r). \tag{3.8}$$

  - The states $\boldsymbol{W}_0^{-,2} = [A^{-,2}, q_l, K_l, A_{0,0}, p_{e,0}]^T$, $\boldsymbol{W}_0^{+,2} = [A^{+,2}, q_r, K_r, A_{0,0}, p_{e,0}]^T$, where $A^{\pm,2}$ satisfy:

$$\frac{\rho}{2}\frac{q_l^2}{(A^{-,2})^2} + K_l\phi\left(\frac{A^{-,2}}{A_{0,0}}\right) + p_{e,0} = \Gamma(\boldsymbol{W}_0^{-,1}), \tag{3.9}$$

$$\frac{\rho}{2}\frac{q_r^2}{(A^{+,2})^2} + K_r\phi\left(\frac{A^{+,2}}{A_{0,0}}\right) + p_{e,0} = \Gamma(\boldsymbol{W}_0^{+,1}). \tag{3.10}$$

  - The states $\boldsymbol{W}_0^{-} = [A^{-}, q_l, K_0, A_{0,0}, p_{e,0}]^T$, $\boldsymbol{W}_0^{+} = [A^{+}, q_r, K_0, A_{0,0}, p_{e,0}]^T$ where $A^{\pm}$ satisfy:

$$\frac{\rho}{2}\frac{q_l^2}{(A^{-})^2} + K_0\phi\left(\frac{A^{-}}{A_{0,0}}\right) + p_{e,0} = \Gamma(\boldsymbol{W}_0^{-,2}), \tag{3.11}$$

$$\frac{\rho}{2}\frac{q_r^2}{(A^{+})^2} + K_0\phi\left(\frac{A^{+}}{A_{0,0}}\right) + p_{e,0} = \Gamma(\boldsymbol{W}_0^{+,2}). \tag{3.12}$$

- The path $\boldsymbol{\Psi}(s)$ connecting the two states is then a reparameterization of the curve composed by:
  1. The arc implicitly defined in the variables A, p_e by:
  $$q = q_l, \quad \frac{\rho}{2}\frac{q_l^2}{A^2} + K_l\phi\left(\frac{A}{A_{0,l}}\right) + p_e = \Gamma(\boldsymbol{W}_l),$$
  that links $\boldsymbol{W}_l$ to the state where $\boldsymbol{W}_0^{-,1}$.
  2. The arc implicitly defined in the variables A, A_0 by:
  $$q = q_l, \quad \frac{\rho}{2}\frac{q_l^2}{A^2} + K_l\phi\left(\frac{A}{A_0}\right) + p_{e,0} = \Gamma(\boldsymbol{W}_0^{-,1}),$$
  that links $\boldsymbol{W}_0^{-,1}$ to $\boldsymbol{W}_0^{-,2}$.
  3. The arc implicitly defined in the variables A, K by:
  $$q = q_l, \quad \frac{\rho}{2}\frac{q_l^2}{A^2} + K\phi\left(\frac{A}{A_0}\right) + p_{e,0} = \Gamma(\boldsymbol{W}_0^{-,2}),$$
  that links $\boldsymbol{W}_0^{-,2}$ to $\boldsymbol{W}_0^{-}$.
  4. The straight segment of the plane $K = K_0$, $A_0 = A_{0,0}$, $p_e = p_{e,0}$ linking $\boldsymbol{W}_0^{-}$ to $\boldsymbol{W}_0^{+}$.
  5. The arc implicitly defined in the variables A, K by:
  $$q = q_r, \quad \frac{\rho}{2}\frac{q_r^2}{A^2} + K\phi\left(\frac{A}{A_0}\right) + p_{e,0} = \Gamma(\boldsymbol{W}_0^{+,2}),$$
  that links $\boldsymbol{W}_0^{+}$ to $\boldsymbol{W}_0^{+,2}$.
  6. The arc implicitly defined in the variables A, A_0 by:
  $$q = q_r, \quad \frac{\rho}{2}\frac{q_r^2}{A^2} + K_r\phi\left(\frac{A}{A_0}\right) + p_{e,0} = \Gamma(\boldsymbol{W}_0^{+,1}),$$
  that links $\boldsymbol{W}_0^{+,2}$ to $\boldsymbol{W}_0^{+,1}$.
  7. The arc implicitly defined in the variables A, p_e by:
  $$q = q_r, \quad \frac{\rho}{2}\frac{q_r^2}{A^2} + K_r\phi\left(\frac{A}{A_{0,r}}\right) + p_e = \Gamma(\boldsymbol{W}_r),$$
  that links $\boldsymbol{W}_0^{+,1}$ to the state where $\boldsymbol{W}_r$.

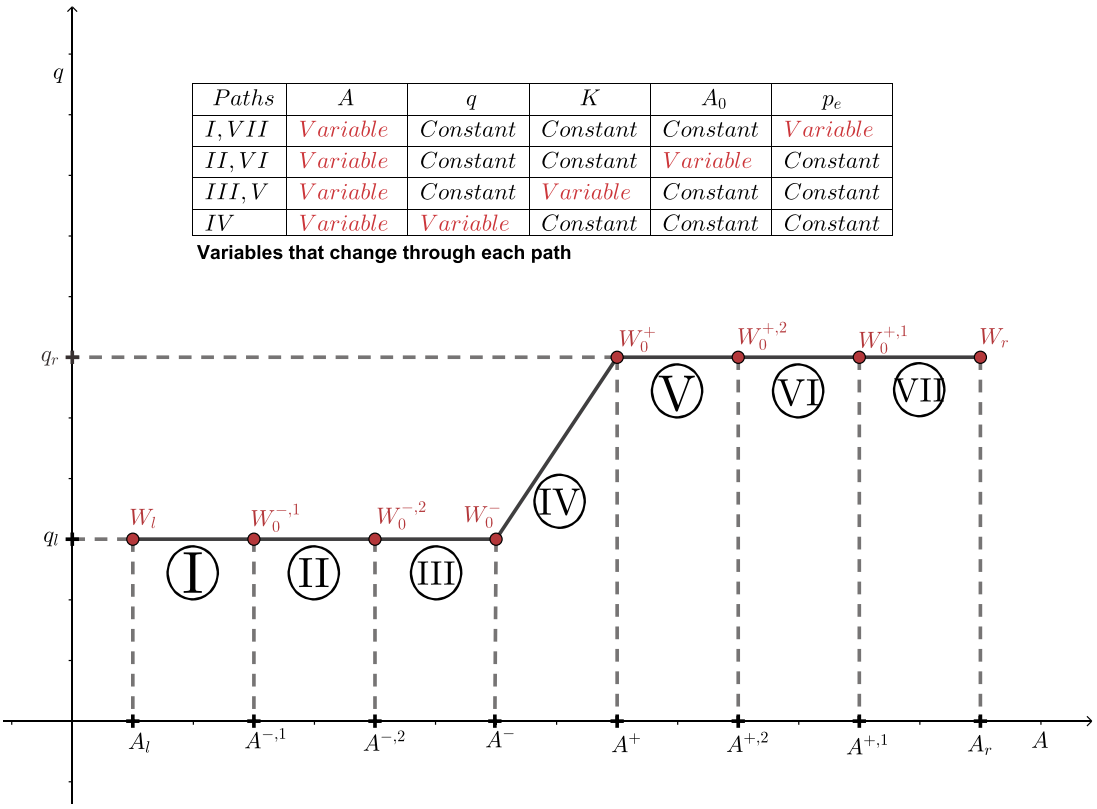

$Paths$	A	q	K	A_0	p_e
I, VII	$Variable$	$Constant$	$Constant$	$Constant$	$Variable$
II, VI	$Variable$	$Constant$	$Constant$	$Variable$	$Constant$
III, V	$Variable$	$Constant$	$Variable$	$Constant$	$Constant$
IV	$Variable$	$Variable$	$Constant$	$Constant$	$Constant$

Variables that change through each path

Fig. 3.1.1. Projection in the (A, q)-plane of the path linking two states $\boldsymbol{W}_l$ and $\boldsymbol{W}_r$. The variables that are constant across every piece are specified.

In Fig. 3.1.1 the projection in the (A, q)-plane of the path linking two states is presented: it is composed of 7 pieces across which only two variables are not constant.

Remark 1. The family of paths so defined satisfies (2.15). In effect, if $\boldsymbol{\sigma}_l = \boldsymbol{\sigma}_r = \boldsymbol{\sigma}$, then $\boldsymbol{\sigma}_0 = \boldsymbol{\sigma}$. In this case, it can be easily checked that A_l solves (3.7), (3.9), (3.11), and A_r solves (3.8), (3.10), (3.12). Therefore,

$$\boldsymbol{W}_0^{-,1} = \boldsymbol{W}_0^{-,2} = \boldsymbol{W}_0^- = \boldsymbol{W}_l, \quad \boldsymbol{W}_0^{+,1} = \boldsymbol{W}_0^{+,2} = \boldsymbol{W}_0^+ = \boldsymbol{W}_r,$$

and the path reduces to the straight segment linking $\boldsymbol{W}_l$ and $\boldsymbol{W}_r$. Therefore

$$\boldsymbol{\Psi}_{\boldsymbol{\sigma}}(s) = \boldsymbol{\sigma}, \quad \forall s \in [0, 1].$$

This definition of path leads to:

$$\int_0^1 \boldsymbol{\mathcal{A}}(\boldsymbol{\Psi}(s))\partial_s \boldsymbol{\Psi}(s)\, ds = \begin{bmatrix} \boldsymbol{F}(\boldsymbol{W}_0^+) - \boldsymbol{F}(\boldsymbol{W}_0^-) \\ 0 \end{bmatrix}. \tag{3.13}$$

In effect, since the path is composed by 7 pieces, there exists a partition

$$0 = s_0 < s_1 < \cdots < s_7 = 1,$$

of the interval $[0, 1]$ such that

$$\boldsymbol{\Psi}(s) = \boldsymbol{\Psi}_j(s), \quad s \in [s_{j-1}, s_j], \quad j = 1, \ldots, 7,$$

where $\boldsymbol{\Psi}_j$ is a parameterization of the jth piece following the order above. Since all the pieces but the fourth are arcs of integral curves of the null eigenvalue one has

$$\mathcal{A}(\boldsymbol{\Psi}_j(s))\partial_s \boldsymbol{\Psi}_j(s) = 0, \quad \forall s \in [s_{j-1}, s_j], \quad \forall j \in \{1, 2, 3, 5, 6, 7\}.$$

Therefore

$$\begin{aligned}\int_0^1 \mathcal{A}(\Psi(s))\partial_s\Psi(s)\,ds &= \int_{s_3}^{s_4} \mathcal{A}(\Psi_4(s))\partial_s\Psi_4(s)\,ds \\ &= \begin{bmatrix} \int_{s_3}^{s_4} \left(\boldsymbol{J}(\Psi_4(s))\partial_s\Psi_{4,\boldsymbol{U}}(s) + \boldsymbol{S}(\Psi_4(s))\partial_s\Psi_{4,\boldsymbol{\sigma}}(s)\right) ds \\ 0 \end{bmatrix} \\ &= \begin{bmatrix} [\boldsymbol{F}(\boldsymbol{W}_0^+) - \boldsymbol{F}(\boldsymbol{W}_0^-) \\ 0 \end{bmatrix}.\end{aligned}$$

To obtain the last equality, we have taken into account that the fourth piece is a segment linking the states $\boldsymbol{W}_0^{\pm} = [\boldsymbol{U}_0^{\pm}, \boldsymbol{\sigma}_0]^T$ so that

$$\boldsymbol{\Psi}_{\boldsymbol{\sigma},4}(s) = \boldsymbol{\sigma}_0, \quad \forall s \in [s_3, s_4].$$

Once the paths have been set, the fluctuations are defined as follows:

$$\mathbb{D}^+(\boldsymbol{W}_l, \boldsymbol{W}_r) = F(\boldsymbol{W}_0^+) - \mathbb{F}(\boldsymbol{U}_0^-, \boldsymbol{U}_0^+; \boldsymbol{\sigma}_0), \tag{3.14}$$

$$\mathbb{D}^-(\boldsymbol{W}_l, \boldsymbol{W}_r) = \mathbb{F}(\boldsymbol{U}_0^-, \boldsymbol{U}_0^+; \boldsymbol{\sigma}_0) - F(\boldsymbol{W}_0^-), \tag{3.15}$$

where, $\mathbb{F}(\cdot,\cdot;\cdot)$ is any continuous function such that, for any $\boldsymbol{\sigma}$, $\mathbb{F}(\cdot,\cdot;\boldsymbol{\sigma})$ is a numerical flux consistent with the physical flux

$$\boldsymbol{F}_{\boldsymbol{\sigma}}(\boldsymbol{U}_l, \boldsymbol{U}_r) := \boldsymbol{F}([\boldsymbol{U}_l, \boldsymbol{\sigma}]^T, [\boldsymbol{U}_r, \boldsymbol{\sigma}]^T),$$

i.e. any continuous function satisfying

$$\mathbb{F}(\boldsymbol{U}, \boldsymbol{U}; \boldsymbol{\sigma}) = \boldsymbol{F}_{\boldsymbol{\sigma}}(\boldsymbol{U}, \boldsymbol{U}), \quad \forall \boldsymbol{U}, \boldsymbol{\sigma}.$$

In particular, in this article the HLL numerical flux is considered (see [33]):

$$\mathbb{F}(\boldsymbol{U}_l, \boldsymbol{U}_r, \boldsymbol{\sigma}) = \begin{cases} \boldsymbol{F}(\boldsymbol{W}_l) & \text{if } S_l \geq 0, \\ \dfrac{S_r\boldsymbol{F}(\boldsymbol{W}_l) - S_l\boldsymbol{F}(\boldsymbol{W}_r)}{S_r - S_l} + \dfrac{S_l S_r}{S_r - S_l}(U_r - U_L), & \text{if } S_l < 0 < S_r, \\ \boldsymbol{F}(\boldsymbol{W}_r) & \text{if } S_r \leq 0, \end{cases}$$

where

$$\boldsymbol{W}_l = [\boldsymbol{U}_l, \boldsymbol{\sigma}]^T, \quad \boldsymbol{W}_r = [\boldsymbol{U}_r, \boldsymbol{\sigma}]^T$$

and

$$S_l = \min\{\lambda_1(\boldsymbol{W}_l), \lambda_5(\boldsymbol{W}_r)\}, \quad S_r = \max\{\lambda_1(\boldsymbol{W}_l), \lambda_5(\boldsymbol{W}_r)\}.$$

See the recent work [61] for discussion on wave speed estimates for HLL-type Riemann solvers.

Remark 2. Although formally the path is composed by arcs that link up to 6 intermediate states, in practice it is enough to compute the states $\boldsymbol{W}_0^- = [A^-, q_l, K_0, A_{0,0}, p_{e,0}]^T$, $\boldsymbol{W}_0^+ = [A^+, q_r, K_0, A_{0,0}, p_{e,0}]^T$ by solving the equations:

$$\frac{\rho}{2}\frac{q_l^2}{(A^-)^2} + K_0\phi\left(\frac{A^-}{A_{0,0}}\right) + p_{e,0} = \Gamma(\boldsymbol{W}_l), \tag{3.16}$$

$$\frac{\rho}{2}\frac{q_r^2}{(A^+)^2} + K_0\phi\left(\frac{A^+}{A_{0,0}}\right) + p_{e,0} = \Gamma(\boldsymbol{W}_r), \tag{3.17}$$

to obtain $A^{\pm}$. Therefore we must solve nonlinear equations of the form: find A such that

$$f(A; q_\alpha, \Gamma(\boldsymbol{W}_\alpha), K_0, A_{0,0}, p_{e,0}) = 0, \tag{3.18}$$

where $\alpha = l, r$ and f is given by (2.21). The following strategy has been used to solve them:

- If $q_\alpha = 0$ (*blood-at-rest* case), Newton-Raphson method with A_α as initial seed is applied.

- If $q_\alpha \neq 0$ (general case) we first compute $A_{crit,\alpha}$ by solving the nonlinear equation

$$g(A; K_\alpha, q_\alpha) = 0,$$

where g is given by (2.24). Newton-Raphson method with A_α as initial guess is used. Once $A_{crit,\alpha}$ has been computed, equation (3.18) is solved as follows:
  - If $f(A_{crit,\alpha}) = 0$, then $A_{crit,\alpha}$ is the unique solution of (3.18).
  - If $f(A_{crit,\alpha}) < 0$, then f has two roots: we use then Newton-Raphson method with initial guess $\frac{A_{crit,\alpha}}{2}$ or $2A_{crit,\alpha}$ to obtain the smallest or the largest root, depending on the regime of the state $\boldsymbol{W}_\alpha$.
  - If $f(A_{crit,\alpha}) > 0$, then f has no roots.

  If Newton-Raphson method does not converge or it gives a negative value of A, we use the bisection method in the intervals $[\epsilon, A_{crit,\alpha}]$ or $[A_{crit,\alpha}, M]$ to obtain the smallest or the largest root, depending on the regime of the state $\boldsymbol{W}_\alpha$. In practice we use $\epsilon = 10^{-10}$ and $M = 1$.

Finally, the first-order fully well-balanced scheme reads as follows:

$$\boldsymbol{U}_i^{n+1} = \boldsymbol{U}_i^n - \frac{\Delta t}{\Delta x}\left(\mathbb{D}^-_{i+\frac{1}{2}} + \mathbb{D}^+_{i-\frac{1}{2}}\right), \tag{3.19}$$

where $\mathbb{D}^\pm_{i+\frac{1}{2}} = \mathbb{D}^\pm(\boldsymbol{W}_i^n, \boldsymbol{W}_{i+1}^n)$ are given by (3.14), (3.15).

Let us show why this method is well-balanced regardless of the choice of the numerical flux and intermediate values: if $\boldsymbol{W}_l$ and $\boldsymbol{W}_r$ are such that (3.5)-(3.6) is verified, then the equations to be solved to find $A^\pm$, (3.16) and (3.17), coincide since $q_l = q_r$ and the right-hand sides are equal. Therefore, if this equation has only one solution or if it has more than one but the same criterion is used to select one of them, one has

$$A^- = A^+$$

and, as a consequence,

$$\boldsymbol{U}_0^- = \boldsymbol{U}_0^+ := \boldsymbol{U}_0, \quad \boldsymbol{W}_0^+ = \boldsymbol{W}_0^- = [\boldsymbol{U}_0, \boldsymbol{\sigma}_0]^T := \boldsymbol{W}_0.$$

Therefore one has

$$\mathbb{F}(\boldsymbol{U}_0^-, \boldsymbol{U}_0^+; \boldsymbol{\sigma}_0) = \mathbb{F}(\boldsymbol{U}_0, \boldsymbol{U}_0; \boldsymbol{\sigma}_0) = \boldsymbol{F}(\boldsymbol{W}_0),$$

and

$$\boldsymbol{F}(\boldsymbol{W}_0^\pm) = \boldsymbol{F}(\boldsymbol{W}_0).$$

Then, taking into account the definition of the fluctuations (3.14)-(3.15), we have

$$\mathbb{D}^\pm(\boldsymbol{W}_l, \boldsymbol{W}_r) = 0,$$

so that the method is well-balanced according to Definition 2.

3.2. Choice of the intermediate values

Choice of $p_{e,0}$

Equations (3.7), (3.8) have the form: find A such that:

$$\frac{\rho}{2}\frac{C^2}{A^2} + K\phi\left(\frac{A}{A_0}\right) + \tilde{p_e} = \Gamma, \tag{3.20}$$

where ρ, K, A_0, C, Γ are given. Let us study their solution depending on the value of $\tilde{p_e}$. To do this, we define the function:

$$p_e(A) = \Gamma - \frac{\rho}{2}\frac{C^2}{A^2} - K\phi\left(\frac{A}{A_0}\right). \tag{3.21}$$

One has:

- $\lim_{A \longrightarrow 0^+} p_e(A) = -\infty$.
- $\lim_{A \longrightarrow +\infty} p_e(A) = -\infty$.

- $p_e'(A) = 0 \iff KA^2\left(m\left(\frac{A}{A_0}\right)^m - n\left(\frac{A}{A_0}\right)^n\right) = \rho C^2$.
  If we consider the function

$$h(A) = KA^2\left(m\left(\frac{A}{A_0}\right)^m - n\left(\frac{A}{A_0}\right)^n\right),$$

  one has:
  – $\lim_{A\longrightarrow 0^+} h(A) = 0$.
  – $\lim_{A\longrightarrow +\infty} h(A) = +\infty$.
  – $h'(A) > 0$, $\forall A > 0$.
  Then h is strictly increasing and there is a unique state A_{crit} such that $h(A_{crit}) = \rho C^2$ that corresponds to a maximum of $p_e(A)$. It can be checked that the corresponding flow is critical.

As a conclusion we have that equation (3.20) has:

- Two solutions if $\tilde{p_e} < p_e(A_{crit})$: A_{sup} that corresponds to a supercritical flow and A_{sub} that corresponds to a subcritical flow.
- One solution if $\tilde{p_e} = p_e(A_{crit})$ that corresponds to a critical flow.
- No solution if $\tilde{p_e} > p_e(A_{crit})$.

In the particular case of equation (3.7), one has $K = K_l$, $A_0 = A_{0,l}$, $\tilde{p_e} = p_{e,0}$, $C = q_l$, and

$$\Gamma = \frac{\rho}{2}\frac{q_l^2}{A_l^2} + K_l\phi\left(\frac{A}{A_{0.l}}\right) + p_{e,l},$$

so that, by definition of p_e,

$$p_{e,l} = p_e(A_l).$$

Therefore, if $p_{e,0}$ is such that $p_{e,0} \leq p_{e,l}$ one has

$$p_{e,0} \leq p_{e,l} = p_e(A_l) \leq p_e(A_{crit})$$

and the equation has always a solution. Similarly, (3.8) has always a solution if $p_{e,0} \leq p_{e,r}$. Therefore we select

$$p_{e,0} = \min(p_{e,l}, p_{e,r}).$$

Choice of $A_{0,0}$

Equations (3.9), (3.10) have the form: find A such that

$$\frac{\rho}{2}\frac{C^2}{A^2} + K\phi\left(\frac{A}{\tilde{A_0}}\right) + p_e = \Gamma, \tag{3.22}$$

where ρ, K, p_e, C, Γ are given. Let us study now their solution depending on the value of $\tilde{A_0}$. To do this, we define the function

$$A_0(A) = \frac{A}{\phi^{-1}(z(A))}, \tag{3.23}$$

where ϕ^{-1} is the inverse of ϕ and

$$z(A) = \frac{\Gamma - p_e - \frac{\rho C^2}{2A^2}}{K}.$$

We have the following:

- $\lim_{A\longrightarrow +\infty} A_0(A) = +\infty$.
- $\lim_{A\longrightarrow 0^+} A_0(A) = 0$. To show this, let us use the variable $B = \phi^{-1}(z(A))$. Since $B \longrightarrow 0^+$ as $A \longrightarrow 0^+$, and $A = \sqrt{\rho/2}|C|(\Gamma - p_e - K\phi(B))^{-\frac{1}{2}}$, one has:

$$\lim_{A\longrightarrow 0^+} A_0(A) = \sqrt{\rho/2}|C| \lim_{B\longrightarrow 0^+} \frac{(\Gamma - p_e - K\phi(B))^{-\frac{1}{2}}}{B}$$
$$= \sqrt{\rho/2}|C| \lim_{B\longrightarrow 0^+} \frac{\left(\frac{\Gamma - p_e - K\phi(B)}{KB^n}\right)^{-\frac{1}{2}} (KB)^{-\frac{n}{2}}}{B} = +\infty,$$

where we have used that

$$\lim_{B\longrightarrow 0^+} \frac{\Gamma - p_e - K\phi(B)}{KB^n} = 1,$$

and $\frac{n}{2} - 1 < 0$ for $n > -2$.

- $A_0'(A) = 0 \iff A^2\phi^{-1}(z(A))\phi'(\phi^{-1}(z(A))) = \frac{\rho C^2}{K} \iff B\phi'(B) + 2\phi(B) = \frac{2}{K}(\Gamma - p_e)$, where $B = \phi^{-1}(z(A))$ again. If we consider the function

  $$j(B) = B\phi'(B) + 2\phi(B),$$

  one has:
  - $\lim_{B\longrightarrow 0^+} j(B) = -\infty$.
  - $\lim_{B\longrightarrow +\infty} j(B) = +\infty$.
  - $j'(B) > 0$, $\forall A > 0$.

  Therefore j is strictly increasing function and there is a unique state B^* such that $j(B^*) = \frac{2}{K}(\Gamma - p_e)$ that corresponds to the minimum $A_{crit} = \sqrt{\rho/2}|C|(\Gamma - p_e - K\phi(B^*))^{-\frac{1}{2}}$ of $A_0(A)$. It can be checked that the corresponding flow is critical.

As a conclusion we have that equation (3.22) has:

- Two solutions if $\tilde{A_0} > A_0(A_{crit})$: A_{sup} that corresponds to a supercritical flow and A_{sub} that corresponds to a subcritical flow.
- One solution if $\tilde{A_0} = A_0(A_{crit})$ that corresponds to a critical flow.
- No solution if $\tilde{A_0} < A_0(A_{crit})$.

By reasoning as in the choice of $p_{e,0}$, we select

$$A_{0,0} = \max(A_{0,l}, A_{0,r}).$$

Choice of K_0

Following [43] K_0 is selected as follows:

- $K_0 = \max(K_l, K_r)$, if $A_l \leq A_{0,0}$ and $A_r < A_{0,0}$.
- $K_0 = \min(K_l, K_r)$, if $A_l \geq A_{0,0}$ and $A_r \geq A_{0,0}$.
- $K_0 = \frac{K_l + K_r}{2}$, otherwise.

This choice ensures that the equations (3.11) and (3.12) always have a solution.

Choice of the solution

The selection of the intermediate values of the parameters ensures that the equations (3.7)-(3.12) have always at least one solution but, in many cases, there are two, one corresponding to a subcritical flow and the other one corresponding to a supercritical flow: a criterion is thus required to select one or another. When there are two possible solutions for A^- (resp. A^+) and the flow regime corresponding to $\boldsymbol{W}_l$ (resp. $\boldsymbol{W}_r$) is subcritical or supercritical, we select the one that makes that the flow regime corresponding to the pairs of states $(\boldsymbol{W}_l, \boldsymbol{W}_0^-)$ (resp. $(\boldsymbol{W}_0^+, \boldsymbol{W}_r)$) is the same (subcritical or supercritical). If the flow regime corresponding to $\boldsymbol{W}_l$ (resp. $\boldsymbol{W}_r$) is critical, we select the one that makes that the flow regime corresponding to the pair of states $(\boldsymbol{W}_0^-, \boldsymbol{W}_r)$ (resp. $(\boldsymbol{W}_l, \boldsymbol{W}_0^+)$) is the same.

3.3. High-order fully well-balanced reconstruction operator

In order to design high-order well-balanced numerical methods, following the strategy introduced in [14], a standard high-order reconstruction operator is selected, i.e. an operator that, given the cell-averages $\{v_j\}$ of a smooth function $v(x)$, provides a high-order approximation of the function at the cells:

$$\mathbb{Q}_i(x; \{v_j\}_{j\in S_i}) \approx v(x), \quad \forall i,$$

where S_i is the set of indices of the cells belonging to the stencil of the ith cell. MUSCL [63], ENO [32], WENO [35,40], CWENO [36,20,19] are examples of such operators.

On the basis of the selected reconstruction operator, a well-balanced reconstruction procedure is build as follows: given a family of cells values $\{\boldsymbol{U}_i = [A_i, q_i]^T\}$:

1. Apply the standard reconstruction operator to $\{q_i\}$ to obtain

$$\mathbb{Q}_{q,i}(x) = \mathbb{Q}_i(x; \{q_j\}_{j\in S_i}).$$

2. Find, if possible, the steady state solution $U_i^*(x) = [A_i^*(x), q_i]^T$ such that:

$$\frac{1}{\Delta x}\int_{x_{i-\frac{1}{2}}}^{x_{i-\frac{1}{2}}} A_i^*(x)dx = A_i. \tag{3.24}$$

A_i^* is implicitly given by

$$\frac{\rho}{2}\frac{q_i^2}{(A_i^*(x))^2} + K(x)\phi\left(\frac{A_i^*(x)}{A_0(x)}\right) + p_e(x) = \Gamma_i,$$

for some constant Γ_i to be found.

3. Compute the fluctuations $\{v_j\}_{j\in S_i}$ within the stencil S_i:

$$v_j = A_j - \frac{1}{\Delta x}\int_{x_{j-\frac{1}{2}}}^{x_{j+\frac{1}{2}}} A_i^*(x)dx, \quad j \in S_i. \tag{3.25}$$

4. Apply the standard reconstruction operator to $\{v_i\}$ to obtain:

$$\mathbb{Q}_{v,i}(x) = \mathbb{Q}_i(x; \{v_j\}_{j\in S_i}).$$

5. Define:

$$\mathbb{P}_i(x) = \begin{bmatrix} \boldsymbol{P}_i(x) \\ \boldsymbol{\sigma}(x) \end{bmatrix} = \begin{bmatrix} A_i^*(x) + \mathbb{Q}_{v,i}(x) \\ \mathbb{Q}_{q,i}(x) \\ K(x) \\ A_0(x) \\ p_e(x) \end{bmatrix}, \quad \boldsymbol{W}^{\pm}_{i+\frac{1}{2}} = \begin{bmatrix} \boldsymbol{U}^{\pm}_{i+\frac{1}{2}} \\ \boldsymbol{\sigma}^{\pm}_{i+1/2} \end{bmatrix},$$

with

$$\boldsymbol{U}^{-}_{i+\frac{1}{2}} = \boldsymbol{P}_i(x_{i+\frac{1}{2}}), \quad \boldsymbol{U}^{+}_{i+\frac{1}{2}} = \boldsymbol{P}_{i+1}(x_{i+\frac{1}{2}})$$

and

$$\boldsymbol{\sigma}^{\pm}_{i+1/2} = \boldsymbol{\sigma}(x^{\pm}_{i+1/2}).$$

The reconstruction operator $\mathbb{P}_i$ is fully well-balanced in the sense that, if it is applied to the cell averages of a steady state solution $\boldsymbol{U}^*$, then

$$\boldsymbol{P}_i(x) = \boldsymbol{U}^*(x), \quad \forall i, \forall x \in I_i; \quad \boldsymbol{U}^{\pm}_{i+\frac{1}{2}} = \boldsymbol{U}^*(x^{\pm}_{i+1/2}), \quad \forall i.$$

Moreover, it is conservative, i.e.

$$\frac{1}{\Delta x}\int_{x_{i-\frac{1}{2}}}^{x_{i+\frac{1}{2}}} \boldsymbol{P}_i(x)dx = \boldsymbol{U}_i, \quad \text{for all } i,$$

provided that $\mathbb{Q}_i$ is conservative, and it is high-order accurate as long as the involved steady state solutions are smooth (see [17] for details).

If the K, A_0, p_e variables are dropped, the numerical method (3.1) can be written as follows:

$$\frac{d\boldsymbol{U}_i}{dt} = -\frac{1}{\Delta x}\Big(\mathbb{D}^-_{i+\frac{1}{2}} + \mathbb{D}^+_{i-\frac{1}{2}} + \boldsymbol{F}(\boldsymbol{W}^-_{i+1/2}) - \boldsymbol{F}(\boldsymbol{W}^+_{i-1/2}) + \int_{x_{i-\frac{1}{2}}}^{x_{i+\frac{1}{2}}} \boldsymbol{S}(\mathbb{P}_i(x)) \cdot \boldsymbol{\sigma}'(x)dx\Big), \tag{3.26}$$

where now

$$\mathbb{D}^{\pm}_{i+1/2} = \mathbb{D}^{\pm}_{i+1/2}(\boldsymbol{W}^-_{i-1/2}, \boldsymbol{W}^+_{i+1/2}),$$

with $\mathbb{D}^{\pm}_{i+1/2}$ given by (3.14)-(3.15).

It can be checked that, if $\boldsymbol{\sigma}$ is continuous at the intercells $x_{i\pm1/2}$, the numerical method reduces to

$$\frac{d\boldsymbol{U}_i}{dt} = -\frac{1}{\Delta x}\Big(\mathbb{F}_{i+1/2} - \mathbb{F}_{i-1/2} + \int_{x_{i-\frac{1}{2}}}^{x_{i+\frac{1}{2}}} \boldsymbol{S}(\mathbb{P}_i(x)) \cdot \boldsymbol{\sigma}'(x)dx\Big), \tag{3.27}$$

with

$$\mathbb{F}_{i+1/2} = \mathbb{F}(\boldsymbol{U}^-_{i+1/2}, \boldsymbol{U}^+_{i+1/2}; \boldsymbol{\sigma}(x_{i+1/2})).$$

3.4. Quadrature formula

The use of a quadrature formula

$$\int_{x_{i-1/2}}^{x_{i+1/2}} f(x)\,dx \approx \Delta x \sum_{m=1}^{M} \beta_m f(x_i^m)$$

to compute cell averages and the numerical source term may spoil the well-balanced character of the method. To avoid this, the second step of the well-balanced reconstruction procedure is replaced by:

- Find, if possible, the steady state solution $\boldsymbol{U}_i^*(x) = [A_i^*(x), q_i]^T$ such that:

$$\sum_{m=1}^{M} \beta_m A_i^*(x_i^m) = A_i. \tag{3.28}$$

Moreover, before applying the quadrature formula to the integrals in (3.26) it is first equivalently rewritten as follows:

$$\frac{dU_i}{dt} = -\frac{1}{\Delta x}\Big(\mathbb{D}^-_{i+\frac{1}{2}} + \mathbb{D}^+_{i-\frac{1}{2}} + \boldsymbol{F}(\boldsymbol{W}^-_{i+1/2}) - \boldsymbol{F}(\boldsymbol{W}^+_{i-1/2}) - \boldsymbol{F}(\boldsymbol{U}_i^*(x^-_{i+1/2}), \boldsymbol{\sigma}^-_{i+1/2})) + \boldsymbol{F}(\boldsymbol{U}_i^*(x^+_{i-1/2}), \boldsymbol{\sigma}^+_{i-1/2}) + \int_{x_{i-\frac{1}{2}}}^{x_{i+\frac{1}{2}}} \big(\boldsymbol{S}(\mathbb{P}_i^t(x)) - \boldsymbol{S}(\boldsymbol{U}_i^*(x), \boldsymbol{\sigma}(x))\big) \cdot \boldsymbol{\sigma}'(x)dx\Big),$$

where $\boldsymbol{U}_i^*$ is the steady state solution that satisfies (3.28). Then, the quadrature formula is applied:

$$\frac{d\boldsymbol{U}_i}{dt} = -\frac{1}{\Delta x}\Big(\mathbb{D}^-_{i+\frac{1}{2}} + \mathbb{D}^+_{i-\frac{1}{2}} + \boldsymbol{F}(\boldsymbol{W}^-_{i+1/2}) - \boldsymbol{F}(\boldsymbol{W}^+_{i-1/2}) - \boldsymbol{F}(\boldsymbol{U}_i^*(x^-_{i+1/2}), \boldsymbol{\sigma}^-_{i+1/2})) + \boldsymbol{F}(\boldsymbol{U}_i^*(x^+_{i-1/2}), \boldsymbol{\sigma}^+_{i-1/2}) + \Delta x \sum_{m=1}^{M} \beta_m \big(\boldsymbol{S}(\mathbb{P}_i^t(x_i^m)) - \boldsymbol{S}(\boldsymbol{U}_i^*(x_i^m), \boldsymbol{\sigma}(x_i^m))\big) \cdot \boldsymbol{\sigma}'(x_i^m)\Big). \tag{3.29}$$

Observe that, if the initial condition is given by the cell averages $\boldsymbol{U}_i^*$ of a steady state solution $\boldsymbol{U}^*$, then

$$\boldsymbol{U}_i^* = \boldsymbol{P}_i = \boldsymbol{U}^*, \quad \forall i,$$

and it can be easily checked that the right-hand side of (3.29) vanishes.

3.5. Second-order fully well-balanced method

In the particular case of second-order methods, the MUSCL reconstruction operator is chosen and the mid-point rule is selected to compute cell-averages and the numerical source terms. The initial cell-values are then given by

$$\boldsymbol{W}_i^0 = \boldsymbol{W}_0(x_i), \quad \text{for all } i,$$

where $\boldsymbol{W}_0(x)$ is the initial condition.

Let us follow the steps in Section 3.3 in order to obtain $\mathbb{P}_i(x)$:

1. Find the stationary solution

$$\boldsymbol{U}_i^*(x) = \begin{pmatrix} A_i^*(x) \\ q_i \end{pmatrix},$$

such that:

$$A_i^*(x_i) = A_i. \tag{3.30}$$

This stationary solution is characterized by

$$\frac{\rho}{2}\frac{q_i^2}{A_i^*(x)^2} + K(x)\phi\left(\frac{A_i^*(x)}{A_0(x)}\right) + p_e(x) = \frac{\rho}{2}\frac{q_i^2}{A_i^2} + K(x_i)\phi\left(\frac{A_i}{A_0(x_i)}\right) + p_e(x_i) = \Gamma(\boldsymbol{W_i}).$$

2. Compute the fluctuations:

$$v_{i-1} = A_{i-1} - A_i^*(x_{i-1}),$$
$$v_i = A_i - A_i^*(x_i) = 0,$$
$$v_{i+1} = A_{i+1} - A_i^*(x_{i+1}),$$

where the mid-point rule has been used again to compute cell-averages.

3. Apply the *minmod* reconstruction operator $\mathbb{Q}_i$ (see [63]) to q_j and v_j:

$$\mathbb{Q}_{q,i}(x) = q_i + minmod\left(\frac{q_i - q_{i-1}}{\Delta x}, \frac{q_{i+1} - q_i}{\Delta x}\right)(x - x_i),$$
$$\mathbb{Q}_{v,i}(x) = v_i + minmod\left(\frac{v_i - v_{i-1}}{\Delta x}, \frac{v_{i+1} - v_i}{\Delta x}\right)(x - x_i),$$

where

$$minmod(a,b) = \begin{cases} \min\{a,b\} & \text{if } a,b > 0, \\ \max\{a,b\} & \text{if } a,b < 0, \\ 0 & \text{otherwise.} \end{cases}$$

4. Define:

$$\mathbb{P}_i(x) = \begin{bmatrix} \boldsymbol{P}_i(x) \\ \boldsymbol{\sigma}(x) \end{bmatrix} = \begin{bmatrix} A_i^*(x) + \mathbb{Q}_{v,i}(x) \\ \mathbb{Q}_{q,i}(x) \\ K(x) \\ A_0(x) \\ p_e(x) \end{bmatrix}, \quad \boldsymbol{W}^{\pm}_{i+\frac{1}{2}} = \begin{bmatrix} \boldsymbol{U}^{\pm}_{i+\frac{1}{2}} \\ \boldsymbol{\sigma}^{\pm}_{i+1/2} \end{bmatrix},$$

with

$$\boldsymbol{U}^{-}_{i+\frac{1}{2}} = \boldsymbol{P}_i(x_{i+\frac{1}{2}}), \quad \boldsymbol{U}^{+}_{i+\frac{1}{2}} = \boldsymbol{P}_{i+1}(x_{i+\frac{1}{2}})$$

and

$$\boldsymbol{\sigma}^{\pm}_{i+1/2} = \boldsymbol{\sigma}(x^{\pm}_{i+1/2}).$$

Once the well-balanced reconstruction procedure has been defined, the numerical method is given by (3.29) where the mid-point rule is used again to compute the numerical source term. Observe that, in this case, one has:

$$\int_{x_{i-\frac{1}{2}}}^{x_{i+\frac{1}{2}}} \left(\boldsymbol{S}(\mathbb{P}_i^t(x)) - \boldsymbol{S}(\boldsymbol{U}_i^*(x), \boldsymbol{\sigma}(x))\right) \cdot \boldsymbol{\sigma}'(x) dx \approx \Delta x \left(\boldsymbol{S}(\mathbb{P}_i^t(x_i)) - \boldsymbol{S}(\boldsymbol{U}_i^*(x_i), \boldsymbol{\sigma}(x_i))\right) \cdot \boldsymbol{\sigma}'(x_i) = 0. \tag{3.31}$$

Therefore, the scheme reduces to:

$$\frac{d\boldsymbol{W}_i}{dt} = -\frac{1}{\Delta x}\Big(\mathbb{D}_{i+1/2}^- + \mathbb{D}_{i-1/2}^+ + \boldsymbol{F}(\boldsymbol{W}_{i+1/2}^-) - \boldsymbol{F}(\boldsymbol{U}_i^*(x_{i+1/2}^-), \boldsymbol{\sigma}(x_{i+1/2}^-)) + \boldsymbol{F}(\boldsymbol{U}_i^*(x_{i-1/2}^+), \boldsymbol{\sigma}(x_{i-1/2}^+)) - \boldsymbol{F}(\boldsymbol{W}_{i-1/2}^+)\Big). \tag{3.32}$$

The discretization in time is performed with the second-order TVD Runge-Kutta method :

$$\begin{aligned} \boldsymbol{W}_i^{(1)} &= \boldsymbol{W}_i^n + \Delta t L(\boldsymbol{W}_i^n), \\ \boldsymbol{W}_i^{n+1} &= \tfrac{1}{2}\boldsymbol{W}_i^n + \tfrac{1}{2}\boldsymbol{W}_i^{(1)} + \tfrac{1}{2}L(\boldsymbol{W}_i^{(1)}), \end{aligned}$$

where $L(\boldsymbol{W}_i)$ represents the right-hand side of (3.32): see [30].

3.6. Third-order fully well-balanced method

In order to design a third-order method the *CWENO* reconstruction of order 3 (see [36], [19], [20]) will be considered and the two-point Gauss quadrature will be used to compute the initial averages and the integrals coming from the source term, namely:

$$\boldsymbol{W}_i^0 = \frac{1}{2}(\boldsymbol{W}_0(x_{i,1}) + \boldsymbol{W}_0(x_{i,2})), \quad \text{for all } i,$$

where $\boldsymbol{W}_0(x)$ is the initial condition and:

$$x_{i,1} = x_{i-\frac{1}{2}} + \frac{\Delta x}{2}\left(-\sqrt{\frac{1}{3}} + 1\right), \quad x_{i,2} = x_{i-\frac{1}{2}} + \frac{\Delta x}{2}\left(\sqrt{\frac{1}{3}} + 1\right).$$

Again let us follow the steps illustrated Section 3.3 in order to obtain $\mathbb{P}_i(x)$:

1. Find the steady state solution:

$$\boldsymbol{U}_i^*(x) = \begin{pmatrix} A_i^*(x) \\ q_i \end{pmatrix},$$

such that:

$$\frac{1}{2}(A_i^*(x_{i,1}) + A_i^*(x_{i,2})) = A_i.$$

To do this, the following nonlinear system is solved: find $A_{i,1}^*$, $A_{i,2}^*$, Γ_i such that:

$$\begin{cases} \dfrac{\rho}{2}\dfrac{q_i^2}{(A_{i,1}^*)^2} + K(x_{i,1})\phi\left(\dfrac{A_{i,1}^*}{A_0(x_{i,1})}\right) + p_e(x_{i,1}) = \Gamma_i, \\ \dfrac{\rho}{2}\dfrac{q_i^2}{(A_{i,2}^*)^2} + K(x_{i,2})\phi\left(\dfrac{A_{i,2}^*}{A_0(x_{2,1})}\right) + p_e(x_{i,2}) = \Gamma_i, \\ A_{i,1}^* + A_{i,2}^* = 2A_i. \end{cases} \tag{3.33}$$

Once this system has been solved obtaining $A_{i,1}^*$, $A_{i,2}^*$, Γ_i, the sought stationary solution is characterized by $q_i^*(x) = q_i$ and

$$\frac{\rho}{2}\frac{q_i^2}{A_i^*(x)^2} + K(x)\phi\left(\frac{A_i^*(x)}{A_0(x)}\right) + p_e(x) = \Gamma_i, \tag{3.34}$$

for every x.

2. Compute the fluctuations:

$$v_{i-1} = A_{i-1} - \frac{1}{2}\left(A_i^*(x_{i-1,1}) + A_i^*(x_{i-1,2})\right),$$
$$v_i = A_i - \frac{1}{2}\left(A_i^*(x_{i,1}) + A_i^*(x_{i,2})\right),$$
$$v_{i+1} = A_{i+1} - \frac{1}{2}\left(A_i^*(x_{i+1,1}) + A_i^*(x_{i+1,2})\right),$$

   where the two-point Gauss quadrature formula has been used to compute cell-averages.
3. Apply the third-order *CWENO* reconstruction operator $\mathbb{Q}_i$ to q_j and v_j to obtain $\mathbb{Q}_{q,i}(x)$ and $\mathbb{Q}_{v,i}(x)$.
4. Define:

$$\mathbb{P}_i(x) = \begin{bmatrix} \boldsymbol{P}_i(x) \\ \boldsymbol{\sigma}(x) \end{bmatrix} = \begin{bmatrix} A_i^*(x) + \mathbb{Q}_{v,i}(x) \\ \mathbb{Q}_{q,i}(x) \\ K(x) \\ A_0(x) \\ p_e(x) \end{bmatrix}, \quad \boldsymbol{W}^{\pm}_{i+\frac{1}{2}} = \begin{bmatrix} \boldsymbol{U}^{\pm}_{i+\frac{1}{2}} \\ \boldsymbol{\sigma}^{\pm}_{i+1/2} \end{bmatrix},$$

   with

$$\boldsymbol{U}^{-}_{i+\frac{1}{2}} = \boldsymbol{P}_i(x_{i+\frac{1}{2}}), \quad \boldsymbol{U}^{+}_{i+\frac{1}{2}} = \boldsymbol{P}_{i+1}(x_{i+\frac{1}{2}})$$

   and

$$\boldsymbol{\sigma}^{\pm}_{i+1/2} = \boldsymbol{\sigma}(x^{\pm}_{i+1/2}).$$

Remark 3. System (3.33) is solved by using the Newton-Raphson method in order to find the root of:

$$\boldsymbol{G}(A_1, A_2, \Gamma) = 0,$$

where:

$$\boldsymbol{G}(A_1, A_2, \Gamma) = \begin{pmatrix} \frac{\rho}{2}\frac{q_i^2}{(A_1)^2} + K(x_{i,1})\phi\left(\frac{A_1}{A_0(x_{i,1})}\right) + p_e(x_{i,1}) - \Gamma \\ \frac{\rho}{2}\frac{q_i^2}{(A_2)^2} + K(x_{i,2})\phi\left(\frac{A_2}{A_0(x_{2,1})}\right) + p_e(x_{i,2}) - \Gamma \\ A_1 + A_2 - 2A_i \end{pmatrix},$$

considering the initial seed as

$$(A_1^0, A_2^0, \Gamma^0) = \left(A_i, A_i, \frac{\rho}{2}\left(\frac{q_i}{A_i}\right)^2 + K(x_i)\phi\left(\frac{A_i}{A_0(x_i)}\right) + p_e(x_i)\right).$$

Once we have obtained the stationary solution $\boldsymbol{U}_i^*(x) = [A_i^*(x), q_i]^T$, it has to be evaluated at the intercells and at the quadrature points of the stencil. In order to find the value of A_i^* at a point x, the nonlinear equation (3.34) has to be solved. The Newton-Raphson method is used again as explained in Remark 2. As it has been seen in Subsection 2.3, this equation may have two possible solutions corresponding to a subcritical and a supercritical flow regime. The following criterion, aimed to preserve the regime of the flow, is used to select one of them:

- If the flow regime corresponding to $\boldsymbol{U}_i$ is subcritical or supercritical, then the solution that corresponds to the same regime is selected at the intercells and quadrature points of the ith cell.
- If the flow regime corresponding to $\boldsymbol{U}_j$, $j \in S_i$, $j \neq i$, is subcritical or supercritical, then the solution that corresponds to the same regime is selected at the intercells and quadrature points of the jth cell.
- If the flow regime corresponding to $\boldsymbol{U}_i$ is critical, then the solution corresponding to the same flow regime as $\boldsymbol{U}_{i-1}$ (resp. $\boldsymbol{U}_{i+1}$) is selected at $x_{i-1/2}$ and $x_{i,1}$ (resp. $x_{i+1/2}$ and $x_{i,2}$).
- If the flow regime corresponding to $\boldsymbol{U}_j$ is critical, then the solution corresponding to the same flow regime as $\boldsymbol{U}_{j-1}$ (resp. $\boldsymbol{U}_{j+1}$) is selected at $x_{j-1/2}$, x_{j-1} and $x_{j,1}$ (resp. $x_{j+1/2}$, x_{j+1} and $x_{j,2}$).

In the two last items it is assumed that extrema of functions $K(x)$, $A_0(x)$, $p_e(x)$, if any, are placed at the center of some cell: in Subsection 2.3 it has been seen that stationary solutions can only have smooth transitions at points at which one of these functions has an extremum.

Once the well-balanced reconstruction procedure has been defined, the numerical method is given by (3.29) where the two-point Gauss quadrature formula is used again to compute the numerical source term. Therefore, the scheme reads as:

$$\frac{d\boldsymbol{W}_i}{dt} = -\frac{1}{\Delta x}\Big(\mathbb{D}^-_{i+1/2} + \mathbb{D}^+_{i-1/2} + \boldsymbol{F}(\boldsymbol{W}^-_{i+1/2}) - \boldsymbol{F}(\boldsymbol{U}^*_i(x^-_{i+1/2}), \boldsymbol{\sigma}(x^-_{i+1/2})) + \boldsymbol{F}(\boldsymbol{U}^*_i(x^+_{i-1/2}), \boldsymbol{\sigma}(x^+_{i-1/2})) - \boldsymbol{F}(\boldsymbol{W}^+_{i-1/2}) + \frac{\Delta x}{2}\left(\left(\boldsymbol{S}(\mathbb{P}^t_i(x_{i,1})) - \boldsymbol{S}(\boldsymbol{U}^*_i(x_{i,1}), \boldsymbol{\sigma}(x_{i,1}))\right)\cdot\boldsymbol{\sigma}'(x_{i,1}) + \left(\boldsymbol{S}(\mathbb{P}^t_i(x_{i,2})) - \boldsymbol{S}(\boldsymbol{U}^*_i(x_{i,2}), \boldsymbol{\sigma}(x_{i,2}))\right)\cdot\boldsymbol{\sigma}'(x_{i,2})\right)\Big). \tag{3.35}$$

The discretization in time is performed with the third-order TVD Runge-Kutta method:

$$\begin{aligned}
\boldsymbol{W}_i^{(1)} &= \boldsymbol{W}_i^n + \Delta t L(\boldsymbol{W}_i^n),\\
\boldsymbol{W}_i^{(2)} &= \tfrac{3}{4}\boldsymbol{W}_i^n + \tfrac{1}{4}\boldsymbol{W}_i^{(1)} + \tfrac{1}{4}\Delta t L(\boldsymbol{W}_i^{(1)}),\\
\boldsymbol{W}_i^{n+1} &= \tfrac{1}{3}\boldsymbol{W}_i^n + \tfrac{2}{3}\boldsymbol{W}_i^{(2)} + \tfrac{2}{3}L(\boldsymbol{W}_i^{(2)}),
\end{aligned}$$

where $L(\boldsymbol{W}_i)$ represents the right-hand side of (3.35): see [30].

4. Numerical tests

In this section several numerical tests are considered to check the performance of the well-balanced numerical methods introduced in the previous sections. The following numerical methods will be applied here to system (2.11):

- O1_WB_GHR_HLL: first-order fully well-balanced method (3.14)-(3.15) using the HLL numerical flux;
- O2_WB_GHR_HLL: second-order fully well-balanced extension: see Subsection 3.5;
- O3_WB_GHR_HLL: third-order fully well-balanced extension: see Subsection 3.6;
- O1_WB_HR_DOT: first-order method that preserves *blood-at-rest* stationary solutions based on the DOT solver (see [58], [24]);
- O1_non_WB_HLL: first-order standard non well-balanced HLL solver.

Remark 4. In the case of O1_WB_GHR_HLL, O2_WB_GHR_HLL and O3_WB_GHR_HLL we use the nondimensional form (2.19) in order to avoid the reconstruction of quantities whose order of magnitude is close to those of rounding errors. This is particularly important in the third-order case. In practice we select the characteristic values as follows

$$\overline{L} = x_f - x_0, \quad \overline{A} = \frac{\sum_{i=0}^N A_0(x_i)}{N}, \quad \overline{U} = \frac{\sum_{i=0}^N \left|\frac{q_0(x_i)}{A_0(x_i)}\right|}{N}, \quad \overline{K} = \sum_{i=0}^{n_{\text{par}}} K_0(x_i), \quad \overline{p_e} = \sum_{i=0}^{N} p_{e,0}(x_i),$$

$$\overline{T} = \frac{\overline{L}}{\overline{U}}, \quad \overline{\Delta x} = \frac{\Delta x}{\overline{L}}, \quad \overline{t_{\text{fin}}} = t_{\text{fin}}\overline{T},$$

where $[x_0, x_f]$ is the space interval; $W_0 = [A_0, q_0, K_0, A_{0,0}, p_{e,0}]^T$ is the initial condition; N is the number of points of the uniform mesh; t_{fin} is the final time of the simulation.

Although all the methods are stable under the usual restriction

$$\Delta t = CFL\frac{\Delta x}{\max_i\{|\lambda_j(\boldsymbol{W}_i^n)|, \quad j = 1, 5.\}},$$

with $CFL \in (0, 1]$, all the numerical simulations have been run with $CFL = 0.5$ since this value ensures the positivity of the HLL solver: see [11].

4.1. Well-balanced property

The objective of this subsection is to check the well-balanced property of the proposed numerical schemes. We consider a N-point uniform mesh of the spatial interval $[0, L]$ and free boundary conditions. For Tests 1-3 we will consider the following discontinuous stationary solutions:

$$\boldsymbol{W}_0(x)^T = \begin{cases} [A_l, q_l, K_l, A_{0,l}, p_{e,l}]^T & \text{if } x < x_g,\\ [A_r, q_r, K_r, A_{0,r}, p_{e,r}]^T & \text{if } x \geq x_g, \end{cases}$$

where the left and the right values are given in Table 2. The value of m, n, ρ, L, x_g, K_{ref}, $A_{0,ref}$, t_{end} and N, are given in Table 1.

Table 1
Parameters of numerical tests: $m[-]$, $n[-]$, ρ[Kg/m^3], L[m], x_g[m], K_{ref}[Pa], $A_{0,\text{ref}}$[m^2], t_{end}[s], $N[-]$.

Parameters	m	n	ρ	L	x_g	K_{ref}	$A_{0,\text{ref}}$	t_{end}	N
Well-balanced tests									
Test 1	0.5	0	1050	0.2	0.5L	58725.0	3.1353E-4	0.1	100
Test 2-3	10	-1.5	1050	0.2	0.5L	58725.0	3.1353E-4	0.1	100
Test 4-5	0.5	0	1050	5	-	-	-	2	100
Accuracy test									
Test 6	0.5	0	1050	5	-	-	-	0.5	-
Riemann problems									
Test 7	0.5	0	1050	0.2	0.3L	58725.0	3.1353E-4	0.007	100
Test 8	10	-1.5	1050	0.2	0.3L	5.0	1.0E-4	0.025	100
Test 9	10	-1.5	1050	0.5	0.5L	33.3333	2.8274E-5	0.02	100
Test 10	10	-1.5	1050	0.5	0.5L	33.3333	2.8274E-5	0.025	100
Test 11	10	-1.5	1050	0.5	0.5L	33.3333	2.8274E-5	0.05	100
Test 12	10	-1.5	1050	0.5	0.5L	33.3333	2.8274E-5	0.05	100
Test 13	10	-1.5	1050	0.5	0.5L	10.0	1.0E-4	0.03	1000
Test 14	0.5	0	1000	0.4	0.05	1.0	1.0E-4	6.605	1000
Test 15	10	-1.5	1050	0.5	0.5L	10.0	1.0E-4	0.03	1000
Test 16	0.5	0	1050	1	0.5L	-	1.0E-4	10	1000
Collapsed vessels									
Test 17	0.5	0	1050	50	0.2L	-	1.0E-4	4	1000
Critical blockage									
Test 18-19	10	-1.5	1050	0.5	0.5L	100	1.0E-4	0.1	1000

Test 1: blood at rest stationary solution Since the selected states can be linked by a stationary contact discontinuity in which $u = 0$, this test allows us to check the ability of the methods to preserve *blood at rest* stationary solutions. As it can be seen in Table 3, all the well-balanced methods capture the stationary solution with machine precision.

Test 2: stationary solution with $u \neq 0$ The selected states can be linked by a stationary contact discontinuity in which $u \neq 0$. Therefore, this test allows us to check the ability of the methods to preserve moving stationary solutions. As it can be seen in Table 4, only fully well-balanced methods capture the stationary solution with machine precision.

Test 3: perturbed stationary solution with $u \neq 0$ In this test, we consider a perturbation of the stationary solution considered in Test 2: more precisely, the initial condition is given by:

$$\boldsymbol{W}_0^P(x) = \boldsymbol{W}_0(x) + \boldsymbol{\delta}(x)^T,$$

where $\boldsymbol{W}_0(x)$ is given again in Tables 1, 2, and

$$\boldsymbol{\delta}(x) = [0.00001e^{-20000(x-0.05)^2}, 0, 0, 0, 0].$$

In Figs. 4.1.1 and 4.1.2, it can be observed how, once the wave generated by the initial perturbation leaves the domain, the underlying stationary solution is recovered better by the fully well-balanced methods.

Test 4: smooth stationary solution We consider the following initial condition:

$$\boldsymbol{W}_0(x)^T = [A^*(x), q^*(x), K(x), A_0(x), p_e(x)]^T, \tag{4.1}$$

where $\boldsymbol{W}_0(x)$ is the subcritical stationary solution such that

$$A^*(0) = A_l, \quad q^*(0) = A_l u_l,$$

and

$$K(x) = K_l + 100e^{-10(x-2.5)^2}, \quad A_0(x) = A_{0,l} + 0.0001e^{-10(x-2.5)^2}, \; p_e(x) = p_{e,l} + 100e^{-10(x-2.5)^2},$$

where $A_l, u_l, K_l, A_{0,l}, p_{e,l}$ are given in Tables 1, 2. This test is devoted to check the ability of the methods to preserve smooth stationary solutions. As it can be seen in Table 5, only fully well-balanced methods capture the stationary solution with machine precision. Nevertheless, the method that preserves blood-at-rest solutions gives better results than the non well-balanced method.

Table 2
Left-right initial values of Riemann problems: $A_{l,r}$[m^2], $u_{l,r}$[m/s], $K_{l,r}$[Pa], $A_{0,l,r}$[m^2], $p_{e,l,r}$[Pa].

Left values	A_l	u_l	K_l	$A_{0,l}$	$p_{e,l}$
Well-balanced tests					
Test 1	$1.0228A_{0,l}$	0.0	K_{ref}	$2A_{0,\text{ref}}$	9999.15
Test 2-3	$1.0228A_{0,l}$	1.0	K_{ref}	$2A_{0,\text{ref}}$	9999.15
Test 4-5	$2.0456A_{0,l}$	1.0	58725	5E-4	10000
Accuracy test					
Test 6	$2.0456A_{0,l}$	0.0	58725	5E-4	10000
Riemann problems					
Test 7	$1.6A_{0,l}$	1.0	K_{ref}	$0.5A_{0,\text{ref}}$	3999.66
Test 8	$0.9A_{0,l}$	0.0	K_{ref}	$1.1A_{0,\text{ref}}$	1333.22
Test 9	3.2E-5	0.1	K_{ref}	$A_{0,\text{ref}}$	66.661
Test 10	2.9E-5	0.2	K_{ref}	$A_{0,\text{ref}}$	66.661
Test 11	3.42E-5	0.5	K_{ref}	$A_{0,\text{ref}}$	66.661
Test 12	3.1E-5	-0.2	K_{ref}	$A_{0,\text{ref}}$	66.661
Test 13	$1.5A_{0,l}$	0.6	$5K_{\text{ref}}$	$A_{0,\text{ref}}$	0.0
Test 14	$0.01A_{0,l}$	2.353043016E-2	$0.919219K_{\text{ref}}$	$A_{0,\text{ref}}$	0.0
Test 15	$1.5A_{0,l}$	1.8	$5K_{\text{ref}}$	$1.1A_{0,\text{ref}}$	66.661
Test 16	1E-6	0.023530423	0.919219	$A_{0,\text{ref}}$	0.0
Collapsed vessels					
Test 17	1E-5	1.323213	0.290682	$A_{0,\text{ref}}$	0.0
Critical blockage					
Test 18	$A_{0,l}$	0.0	K_{ref}	$A_{0,\text{ref}}$	0.0
Test 19	$A_{0,l}$	0.0	K_{ref}	$A_{0,\text{ref}}$	0.0

Right values	A_r	u_r	K_r	$A_{0,r}$	$p_{e,r}$
Well-balanced tests					
Test 1	$0.9977A_{0,r}$	0.0	$10K_{\text{ref}}$	$A_{0,\text{ref}}$	11332.37
Test 2-3	3.109988E-4	2.06224886	$10K_{\text{ref}}$	$A_{0,\text{ref}}$	11332.37
Test 4-5	-	-	-	-	-
Accuracy test					
Test 6	-	-	-	-	-
Riemann problems					
Test 7	$1.05A_{0,r}$	0.0	$10K_{\text{ref}}$	$A_{0,\text{ref}}$	0.0
Test 8	$1.6A_{0,r}$	0.0	$10K_{\text{ref}}$	$1.3A_{0,\text{ref}}$	666.61
Test 9	3.2E-5	0.2	K_{ref}	$1.1A_{0,\text{ref}}$	66.661
Test 10	3.2E-5	0.1	$100K_{\text{ref}}$	$1.05A_{0,\text{ref}}$	66.661
Test 11	3.34E-5	-0.1	$40K_{\text{ref}}$	$1.15A_{0,\text{ref}}$	66.661
Test 12	3.1E-5	0.1	$30K_{\text{ref}}$	$1.05A_{0,\text{ref}}$	66.661
Test 13	$1.1A_{0,r}$	1.5	$50K_{\text{ref}}$	$A_{0,\text{ref}}$	0.0
Test 14	$0.01243004A_{0,r}$	2.25423876E-2	$0.781336K_{\text{ref}}$	$A_{0,\text{ref}}$	0.0
Test 15	$1.1A_{0,r}$	2.0	$50K_{\text{ref}}$	$1.2A_{0,\text{ref}}$	6.6661
Test 16	1E-5	0.022542384	0.781336	$A_{0,\text{ref}}$	0.0
Collapsed vessels					
Test 17	1.2429978E-6	7.3158749	0.247	$A_{0,\text{ref}}$	666.612
Critical blockage					
Test 18	$A_{0,r}$	0.0	K_{ref}	$A_{0,\text{ref}}$	-200
Test 19	$A_{0,r}$	0.0	K_{ref}	$A_{0,\text{ref}}$	-2000

Table 3
Test 1: L^1 errors at time $t = 0.1$.

Scheme	$\|\|\Delta A\|\|_1$	$\|\|\Delta u\|\|_1$
O1_WB_GHR_HLL	6.56E-20	2.73E-15
O2_WB_GHR_HLL	5.71E-20	8.63E-16
O3_WB_GHR_HLL	5.96E-20	1.49E-15
O1_WB_HR_DOT	5.71E-20	9.52E-15
O1_non_WB_HLL	7.42E-06	0.13

Table 4
Test 2: L^1 errors at time $t = 0.1$.

Scheme	$\|\|\Delta A\|\|_1$	$\|\|\Delta u\|\|_1$
O1_WB_GHR_HLL	1.03E-19	1.26E-14
O2_WB_GHR_HLL	1.03E-19	1.26E-14
O3_WB_GHR_HLL	6.44E-20	3.78E-14
O1_WB_HR_DOT	2.50E-09	2.31E-4
O1_non_WB_HLL	4.52E-06	0.36

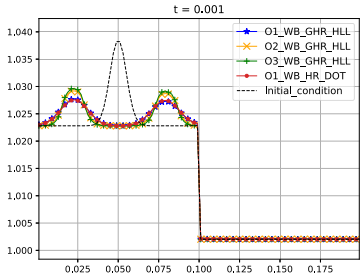

Variable A/A_0. Time $t = 0.001$

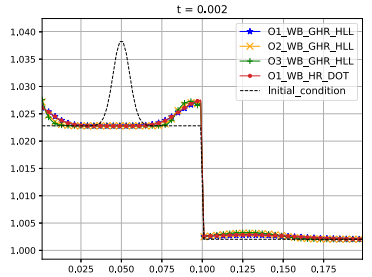

Variable A/A_0. Time $t = 0.002$

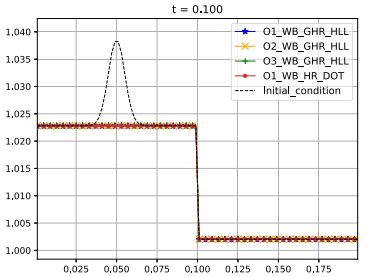

Variable A/A_0. Time $t = 0.1$

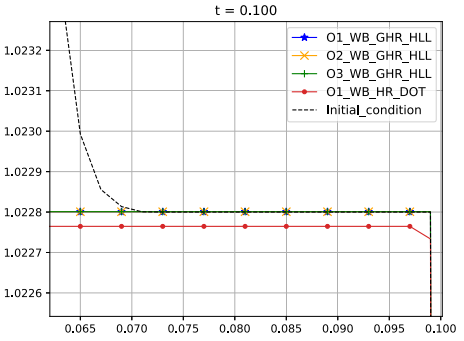

Left zoom. Time $t = 0.1$

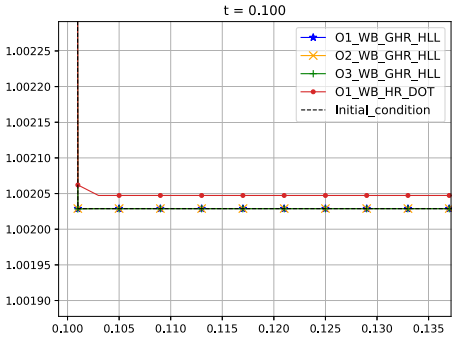

Right zoom. Time $t = 0.1$

Fig. 4.1.1. Test 3: comparison of the numerical solutions and the initial condition. Variable A/A_0. Top: time $t = 0.001$ (left), time $t = 0.002$ (center), time $t = 0.1$ (right). Bottom: left zoom contact discontinuity at time $t = 0.1$ (left), right zoom contact discontinuity at time $t = 0.1$ (right).

Table 5
Test 4: L^1 errors at time $t = 0.1$.

Scheme	$\|\|\Delta A\|\|_1$	$\|\|\Delta u\|\|_1$
O1_WB_GHR_HLL	3.66E-18	3.66E-15
O2_WB_GHR_HLL	3.85E-18	3.84E-15
O3_WB_GHR_HLL	2.94E-18	6.12E-15
O1_WB_HR_DOT	8.37E-12	6.46E-09
O1_non_WB_HLL	1.81E-07	2.73E-3

Test 5: perturbed smooth stationary solution We consider the following initial condition:

$$\boldsymbol{W}_0^P(x) = \boldsymbol{W}_0(x) + \boldsymbol{\delta}(x)^T,$$

where $\boldsymbol{W}_0(x)$ is the subcritical stationary solution considered in Test 4 and

$$\boldsymbol{\delta}(x) = [10^{-7} e^{-40(x-1)^2}, 0, 0, 0, 0].$$

Figs. 4.1.3 and 4.1.4 show the differences between the numerical solutions and the underlying stationary solution at different times. It can be observed that, once the wave generated by the initial perturbation leaves the domain, the stationary solution is exactly recovered only by the fully well-balanced methods. As expected, the evolution of the perturbation is better captured as the order of the method increases.

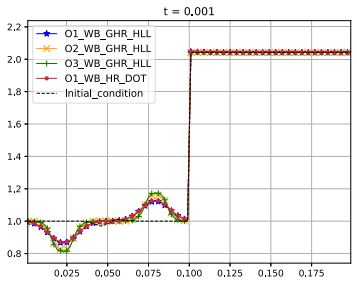

Variable u. Time $t = 0.001$

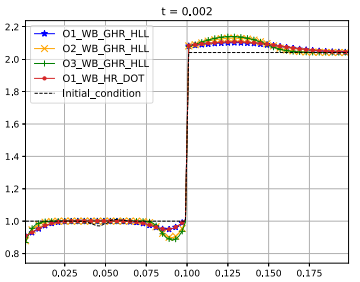

Variable u. Time $t = 0.002$

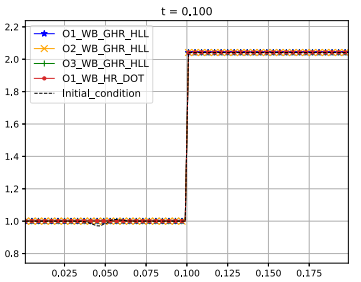

Variable u. Time $t = 0.1$

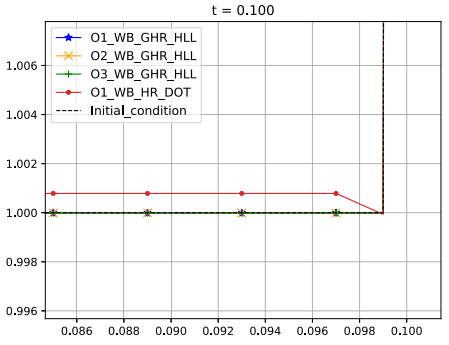

Left zoom. Time $t = 0.1$

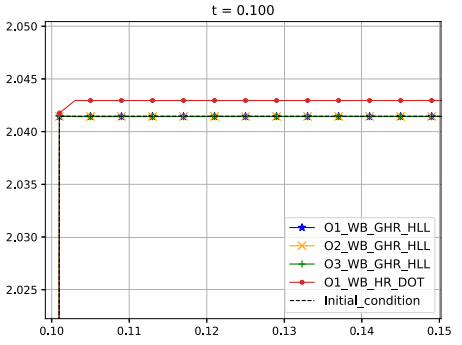

Right zoom. Time $t = 0.1$

Fig. 4.1.2. Test 3: comparison of the numerical and the initial condition. Variable u. Top: time $t = 0.001$ (left), time $t = 0.002$ (center), time $t = 0.1$ (right). Bottom: left zoom contact discontinuity at time $t = 0.1$ (left), right zoom contact discontinuity at time $t = 0.1$ (right).

4.2. Accuracy test

This test is devoted to check the accuracy of the fully well-balanced methods. The selected parameters are given in Tables 1, 2.

Test 6 In this test we consider an initial condition that represents a perturbation of a blood at rest stationary solution in the same setting as Test 4-5. More precisely, the initial condition is given by:

$$\boldsymbol{W}_0^P(x) = \boldsymbol{W}_0(x) + \delta(x)^T, \tag{4.2}$$

where $\boldsymbol{W}_0(x)$ is the blood at rest solution defined by

$$A^*(0) = A_l, \quad q^* = 0,$$

and

$$K(x) = K_l + 100e^{-10(x-2.5)^2}, \quad A_0(x) = A_{0,l} + 0.0001e^{-10(x-2.5)^2}, \, p_e(x) = p_{e,l} + 100e^{-10(x-2.5)^2},$$

where A_l, K_l, $A_{0,l}$, $p_{e,l}$ are given in Tables 1, 2, and

$$\delta(x) = [10^{-6}e^{-40(x-1)^2}, 0, 0, 0, 0].$$

We use 200-, 400-, 800- and 1600-point uniform meshes in order to compute the errors and check the order of the first-, second- and third-order fully well-balanced schemes. The reference solution has been computed with the third-order fully well-balanced method using a 6400-point uniform grid. In Table 6 we show the results from which we conclude that the expected order of accuracy is obtained in the three cases.

4.3. Riemann problems

We consider again a N-point uniform mesh and free boundary conditions. Let us consider the following Riemann problems:

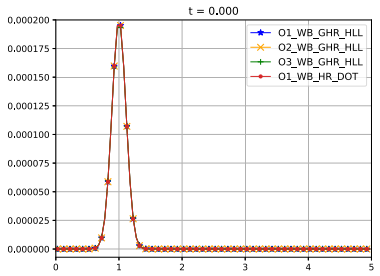

Variable A/A_0. Time $t = 0.0$

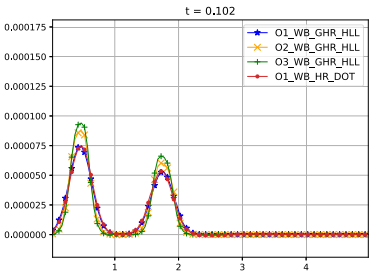

Variable A/A_0. Time $t = 0.1$

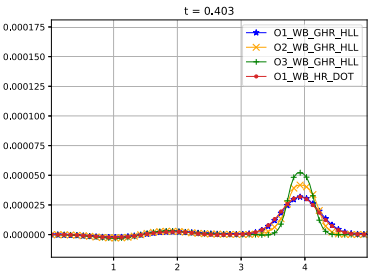

Variable A/A_0. Time $t = 0.4$

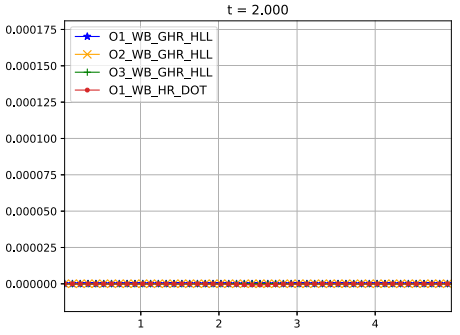

Variable A/A_0. Time $t = 2.0$

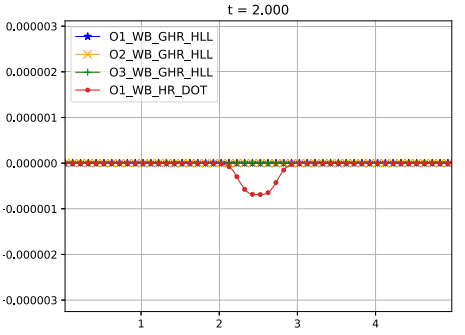

Zoom. Time $t = 2.0$

Fig. 4.1.3. Test 5: plot of the perturbation, i.e., difference between the numerical solution and the initial stationary solution. Variable A/A_0. Top: time $t = 0.0$ (left), time $t = 0.1$ (center), time $t = 0.4$ (right). Bottom: time $t = 2$ (left), zoom at time $t = 2$ (right).

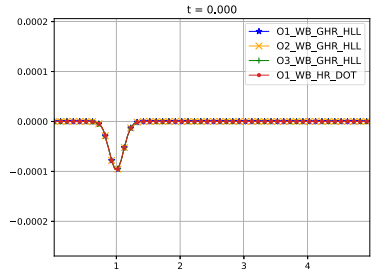

Variable u. Time $t = 0.0$

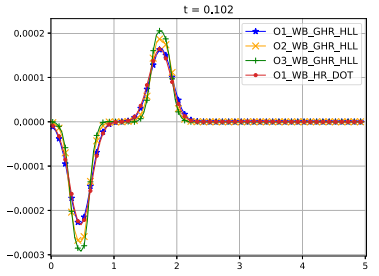

Variable u. Time $t = 0.1$

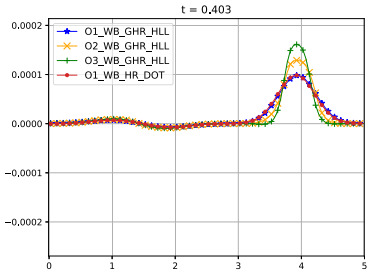

Variable u. Time $t = 0.4$

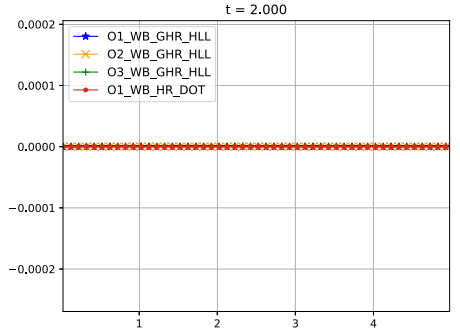

Variable u. Time $t = 2.0$

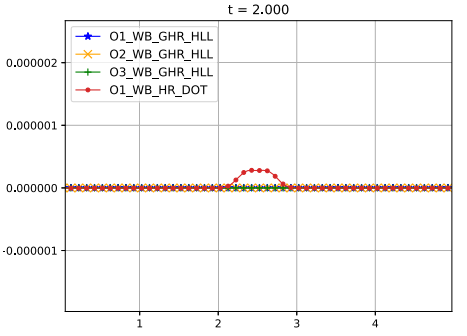

Zoom. Time $t = 0.2$

Fig. 4.1.4. Test 5: plot of the perturbation, i.e., difference between the numerical solution and the initial stationary solution. Variable u. Top: time $t = 0.0$ (left), time $t = 0.1$ (center), time $t = 0.4$ (right). Bottom: time $t = 2$ (left), zoom at time $t = 2$ (right).

Table 6
Test 6: order of accuracy for the first-, second- and third-order fully well-balanced scheme: L^1 errors $||\Delta \cdot ||_1$ at time $t = 0.5$.

First-order				
Number of cells	$\|\|\Delta A\|\|_1$	Order	$\|\|\Delta u\|\|_1$	Order
200	1.51E-07	-	5.92E-04	-
400	7.86E-08	0.95	4.01E-04	0.56
800	4.34E-08	0.86	2.48E-04	0.69
1600	2.38E-08	0.87	1.42E-04	0.80
Second-order				
Number of cells	$\|\|\Delta A\|\|_1$	Order	$\|\|\Delta u\|\|_1$	Order
200	8.87E-08	-	1.98E-04	-
400	2.33E-08	1.93	5.66E-05	1.81
800	5.87E-09	1.99	1.45E-05	1.97
1600	1.47E-09	2.00	3.65E-06	1.99
Third-order				
Number of cells	$\|\|\Delta A\|\|_1$	Order	$\|\|\Delta u\|\|_1$	Order
200	2.32E-08	-	1.44E-04	-
400	4.20E-09	2.47	2.60E-05	2.47
800	4.59E-10	3.19	2.83E-06	3.20
1600	3.63E-11	3.66	2.22E-07	3.68

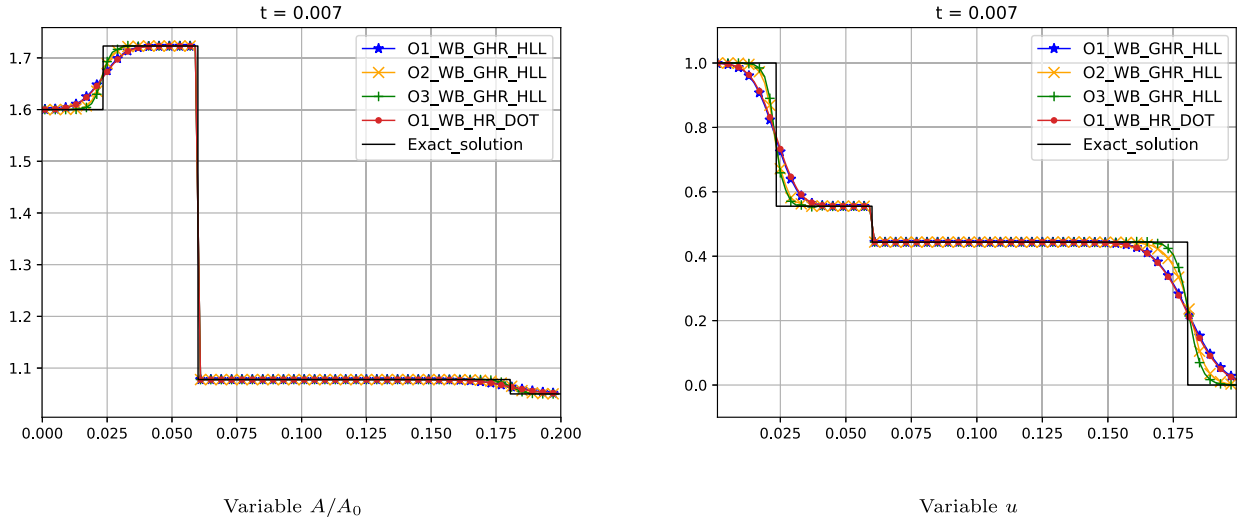

Fig. 4.3.1. Test 7: comparison of the numerical and the exact solutions: variables A/A_0 (left) and u (right).

$$\boldsymbol{W}_0(x)^T = \begin{cases} [A_l, q_l, K_l, A_{0,l}, p_{e,l}]^T & \text{if } x < x_g, \\ [A_r, q_r, K_r, A_{0,r}, p_{e,r}]^T & \text{if } x \geq x_g, \end{cases}$$

where the left and the right values are given in Table 2. The value of m, n, ρ, L, x_g, K_{ref}, $A_{0,ref}$, t_{end} and N, are given in Table 1.

Test 7-12 The numerical results for these subcritical test cases, taken from [58], are shown in Figs. 4.3.1–4.3.6: as it can be seen, both the fully well-balanced methods and the method that preserves blood-at-rest solutions capture correctly the exact solution while, as expected, the second- and third-order ones give better results. Here we describe the wave pattern of the solution of each Riemann problem:

- **Test 7**: the solution consists of a left shock and a right shock traveling in opposite directions and separated by a stationary contact discontinuity in an artery. It represents the problem of a systolic pressure and flow peak arriving to a certain region of the thoracic aorta. Moreover, it is chosen to compress the proximal portion of the aorta, i.e., the part that was already reached by the systolic peak.
- **Test 8**: the solution consists of a left shock and a right rarefaction traveling in opposite directions and separated by a stationary contact discontinuity in a vein. It describes the problem of an internal jugular vein during a Valsalva ma-

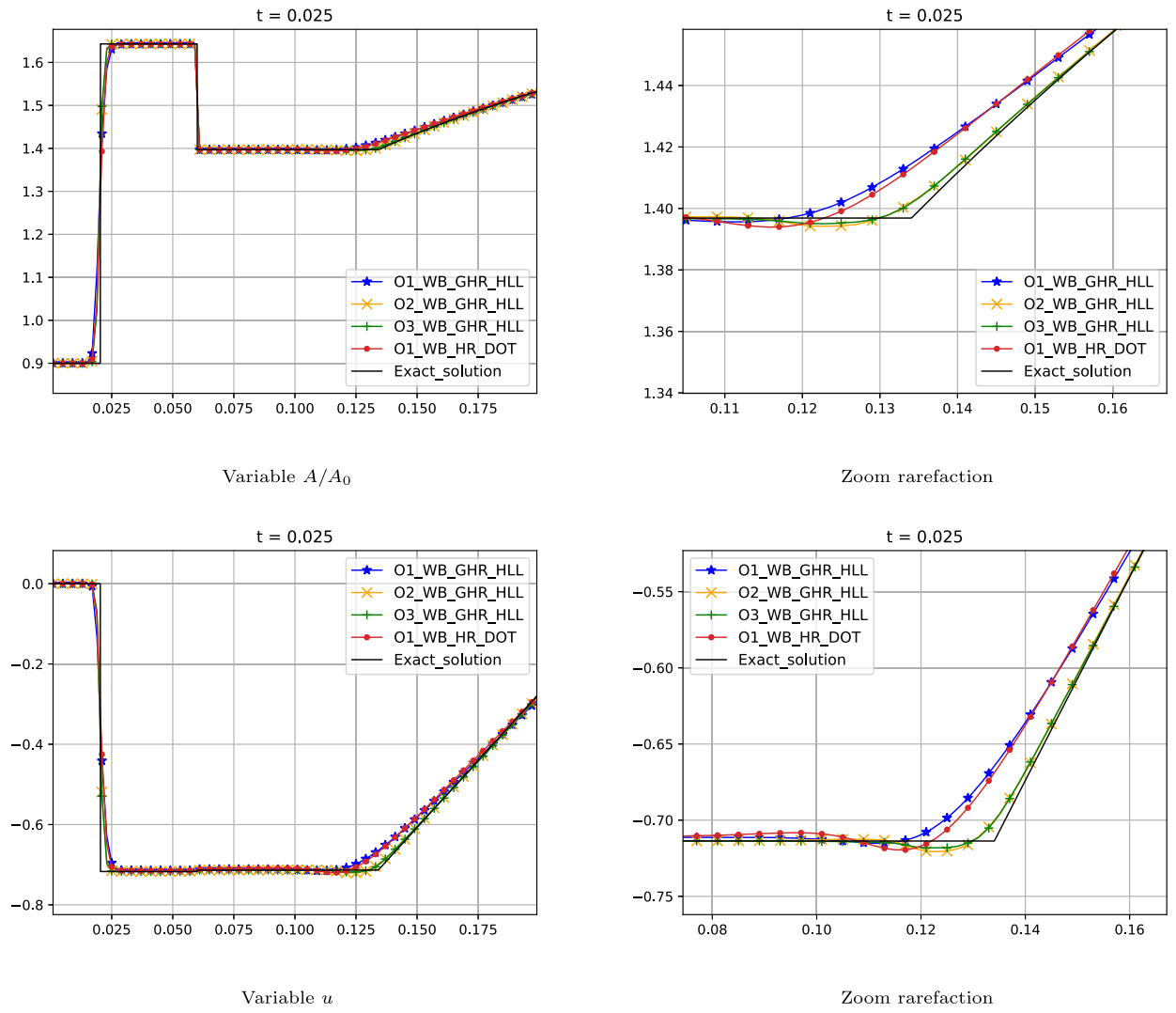

Fig. 4.3.2. Test 8: comparison of the numerical and the exact solutions. Top: variable A/A_0 (left) and zoom rarefaction (right). Bottom: variable u (left) and zoom rarefaction (right).

neuver in which the subject exhales while closing all airways. This maneuver produces a high central venous pressure, reaching values around 40mmHg. In this idealized problem setup, we consider the case in which the valve presented at the proximal end, relative to heart, of the internal jugular vein, suddenly fails to fulfill its function of preventing venous reflux toward the head. The negative pressure as initial condition corresponds to a standing subject.

- **Test 9**: the solution consists of a left rarefaction and a right shock traveling in opposite directions and separated by a stationary contact discontinuity in a vein.
- **Test 10**: the solution consists of a left shock and a right rarefaction traveling in opposite directions and separated by a stationary contact discontinuity in a vein.
- **Test 11**: the solution consists of a left shock and a right shock traveling in opposite directions and separated by a stationary contact discontinuity in a vein.
- **Test 12**: the solution consists of a left rarefaction and a right rarefaction traveling in opposite directions and separated by a stationary contact discontinuity in a vein.

Test 13 In this test, taken from [43], the differences between the fully well-balanced methods and the one that only preserves blood-at-rest stationary solutions are clearer: only the numerical results obtained with the former seem to converge to the exact solution. To see this, we show the numerical results in a fine mesh of 1000 points: see Fig. 4.3.7. The solution consists of a left rarefaction and a right rarefaction separated by a stationary contact discontinuity in a vein.

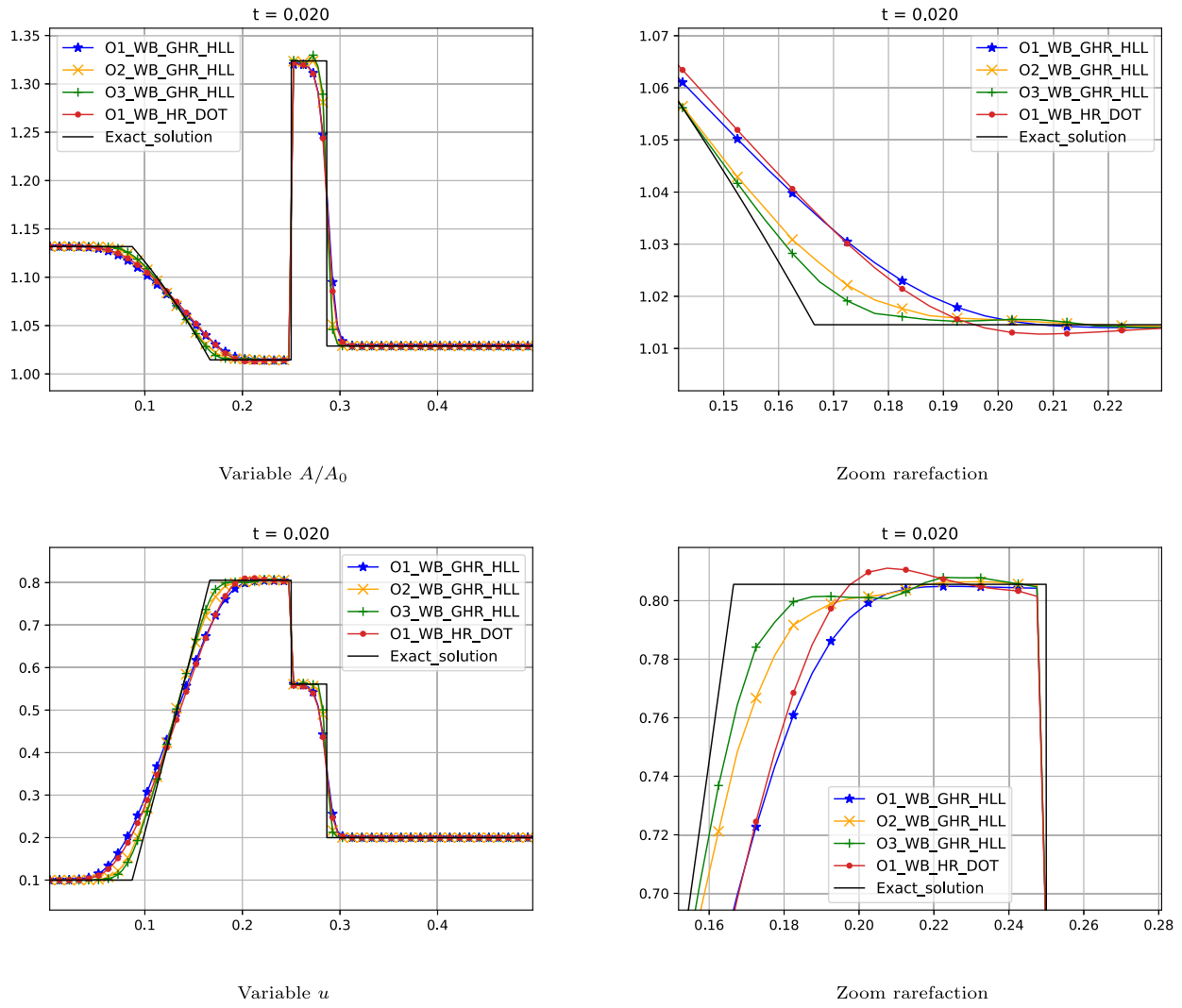

Fig. 4.3.3. Test 9: comparison of the numerical and the exact solutions. Top: variable A/A_0 (left) and zoom rarefaction (right). Bottom: variable u (left) and zoom rarefaction (right).

Test 14 In this test case, taken from [49], a Riemann problem whose initial states are supercritical is considered. The solution consists of a stationary contact discontinuity followed by a left rarefaction wave and a right rarefaction wave in an artery. Fig. 4.3.8 shows again the numerical results obtained using a mesh of 1000 points. The differences between the fully well-balanced methods and the one that only preserves blood-at-rest stationary solutions are also clear in this case: only the numerical results obtained with the former capture correctly the intermediate states.

Test 15 We consider now a Riemann problem in which all the variables are discontinuous in the initial condition. The solution consists of a left rarefaction followed by a stationary contact discontinuity and a right shock wave in a vein. Once again, fully well-balanced schemes capture correctly the exact solution and, as expected, second- and third-order methods give better results than first-order ones: see Fig. 4.3.9.

Test 16 In this test we consider a Riemann problem that has three different solutions according to [25]. Fig. 4.3.10 shows the numerical results given by the fully well-balanced schemes and the one that only preserves blood-at-rest stationary solutions. As it can be observed all methods seem to capture the "F" wave configuration in [25], which corresponds to a stationary contact discontinuity followed by a left shock wave and a right rarefaction wave in an artery. In fact, according to [56], this configuration would be the physically relevant solution , i.e, the one that satisfies the global entropy condition proposed in [21]. Nevertheless, in the zoom of variables A/A_0 and u in Fig. 4.3.10, it can be observed that only the fully well-balanced methods capture correctly the intermediate state appearing between the stationary contact discontinuity and the 1-shock wave.

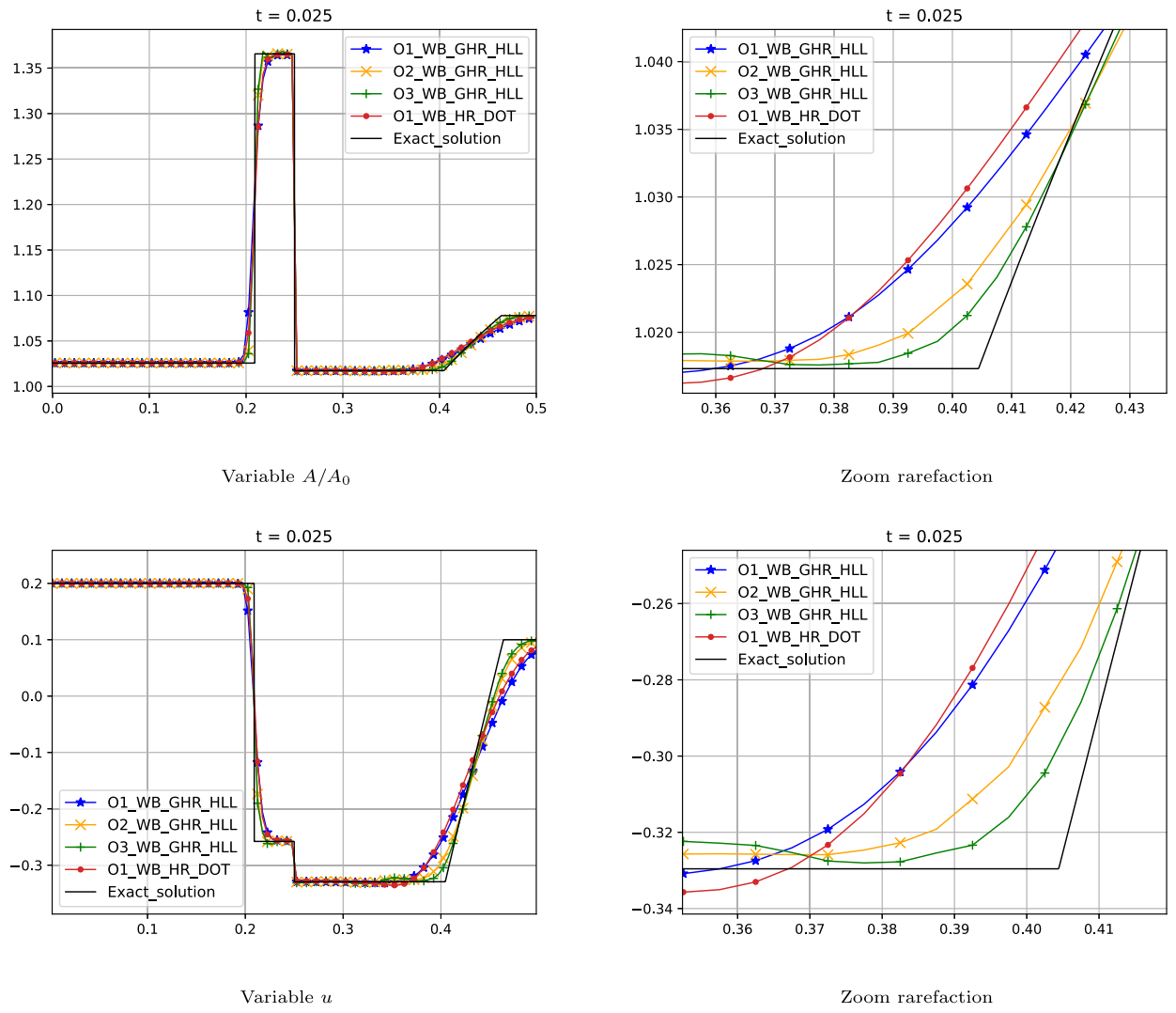

Fig. 4.3.4. Test 10: comparison of the numerical and the exact solutions. Top: variable A/A_0 (left) and zoom rarefaction (right). Bottom: variable u (left) and zoom rarefaction (right).

4.4. Collapsed vessels

The appearance of vacuum states due to vessel collapse has not been specifically considered in this article. Further analysis is required to include this phenomenon in the well-balanced reconstruction procedure, specially in the case of veins. Nevertheless, in order to check if this methodology is able to handle nearly collapsed arteries, the following test case, similar to the one in [49], is considered.

Test 17 This test consists on a supercritical flow in an artery whose solution is given by a stationary contact discontinuity followed by a left rarefaction and a right rarefaction traveling in the same direction. Fig. 4.4.1 shows the numerical results of the fully well-balanced schemes obtained using a mesh of 1000 points. The reference solution has been computed with the first-order fully well-balanced using a fine mesh of 20000 points. We observe that the numerical solutions converge to the reference solution dealing well with the collapsed area.

4.5. Critical blockage

The following two test cases, similar to the ones in [49], are devoted to analyze the numerical solution of the methods when dealing with the transition from subcritical to critical blockage conditions. We observe in Tables 1 and 2 that the initial conditions are the same in both cases except for the variation in the external pressure, which is atmospheric on the left and sub-atmospheric on the right.

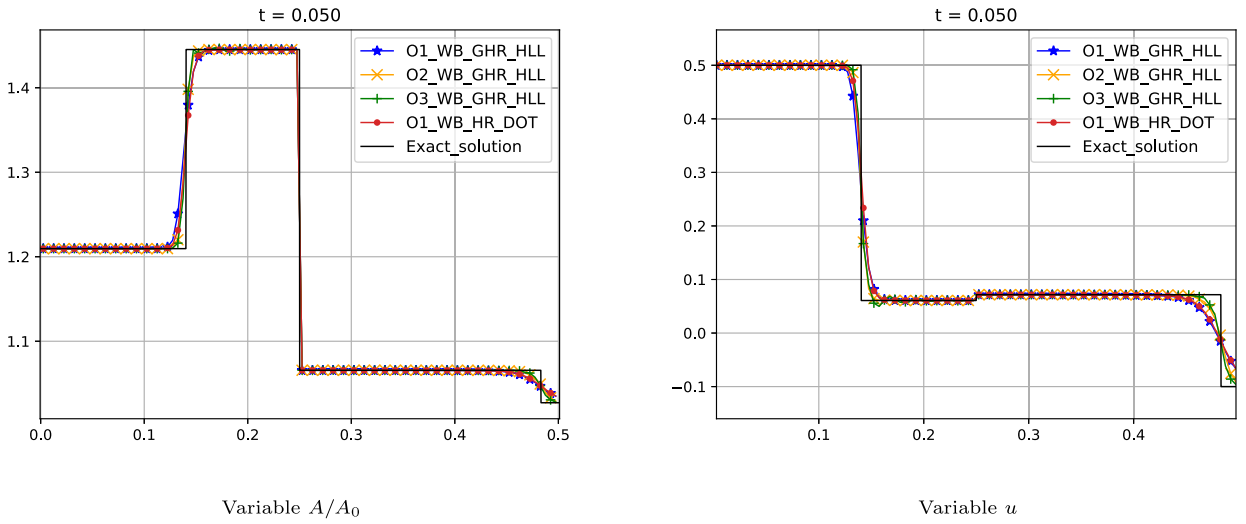

Fig. 4.3.5. Test 11: comparison of the numerical and the exact solutions: variables A/A_0 (left) and u (right).

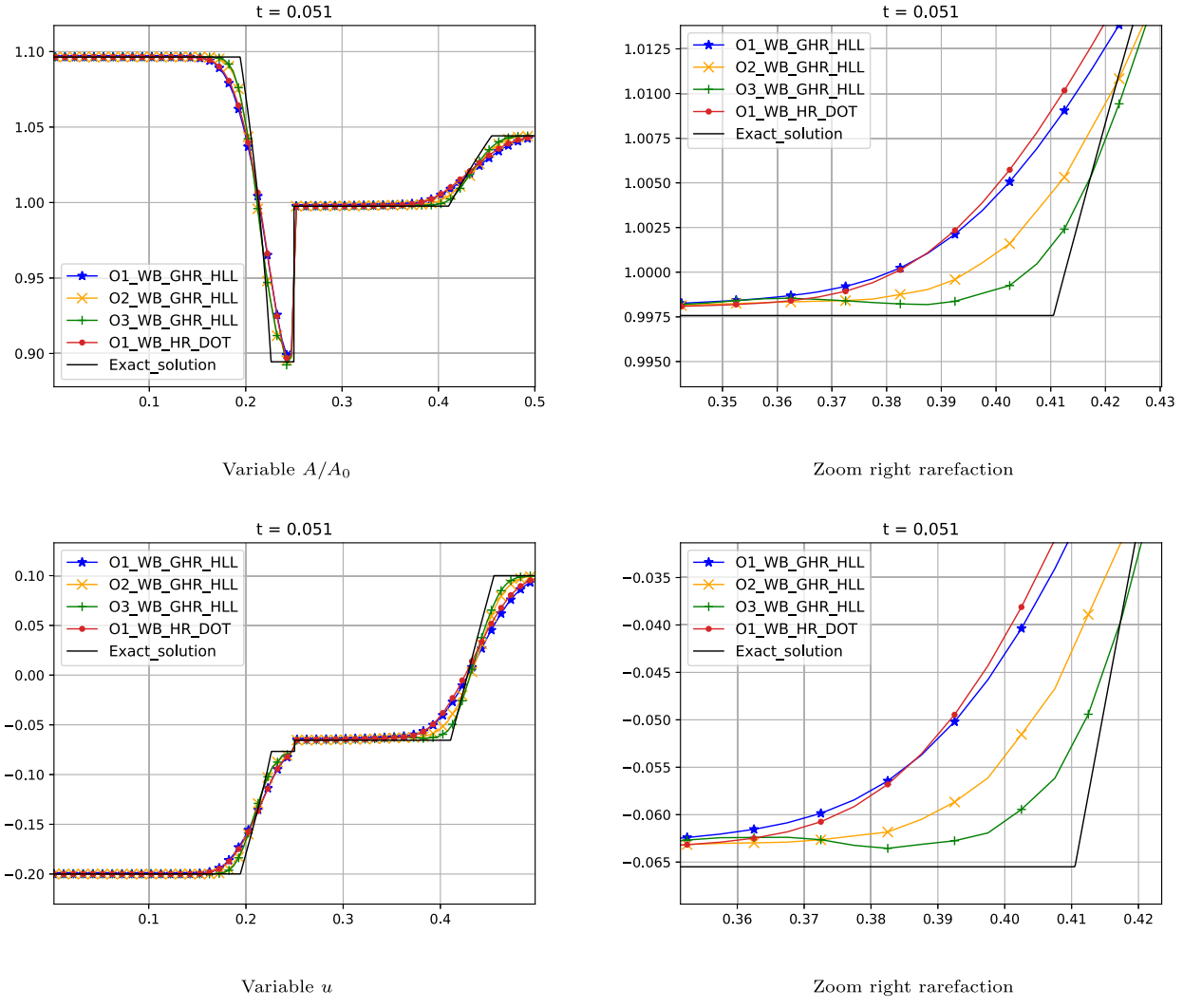

Fig. 4.3.6. Test 12: comparison of the numerical and the exact solutions. Top: variable A/A_0 (left) and zoom right rarefaction (right). Bottom: variable u (left) and zoom right rarefaction (right).

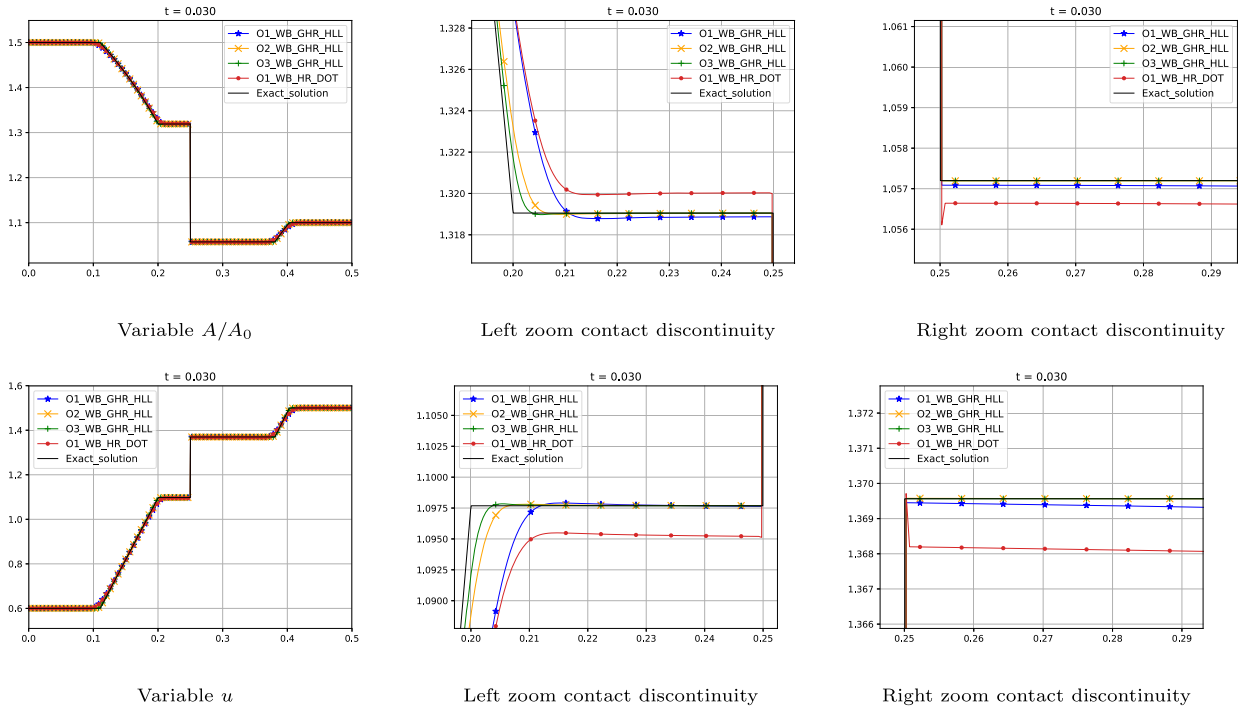

Fig. 4.3.7. Test 13: comparison of the numerical and the exact solutions. Top: variable A/A_0 (left), left zoom contact discontinuity (center), right zoom contact discontinuity (right). Bottom: variable u (left), left zoom contact discontinuity (center), right zoom contact discontinuity (right).

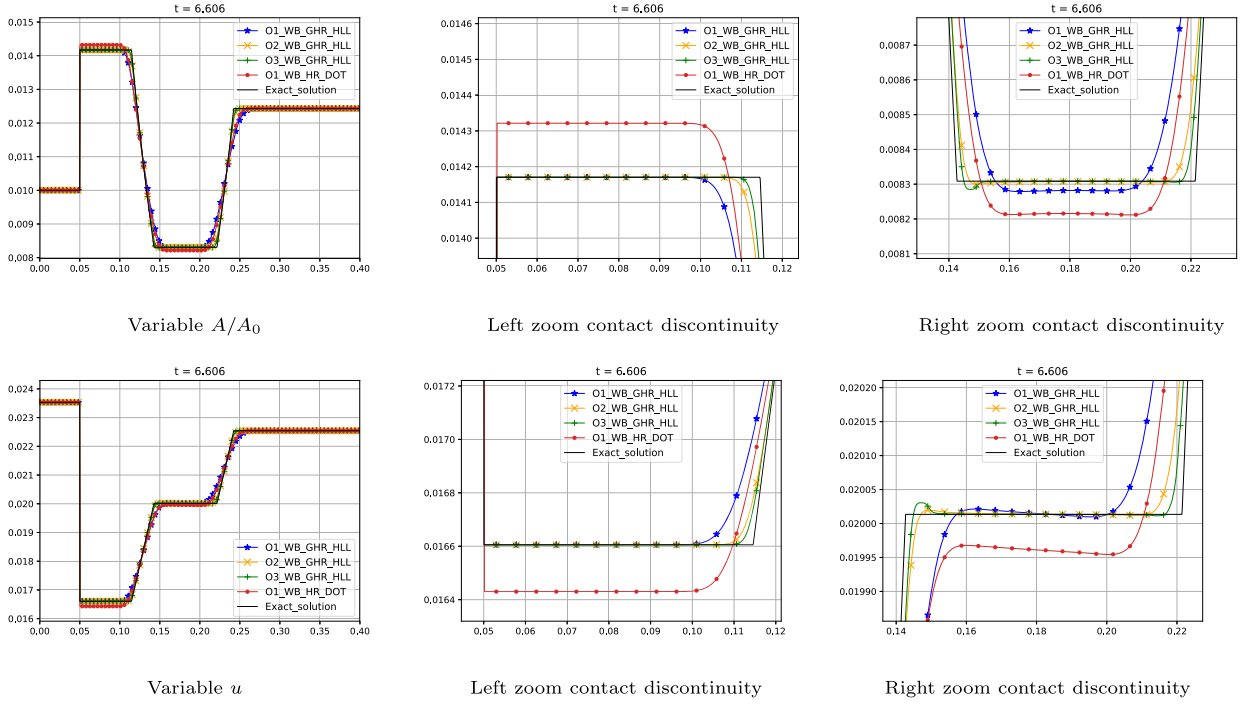

Fig. 4.3.8. Test 14: comparison of the numerical and the exact solutions. Top: variable A/A_0 (left), left zoom contact discontinuity (center), right zoom contact discontinuity (right). Bottom: variable u (left), left zoom contact discontinuity (center), right zoom contact discontinuity (right).

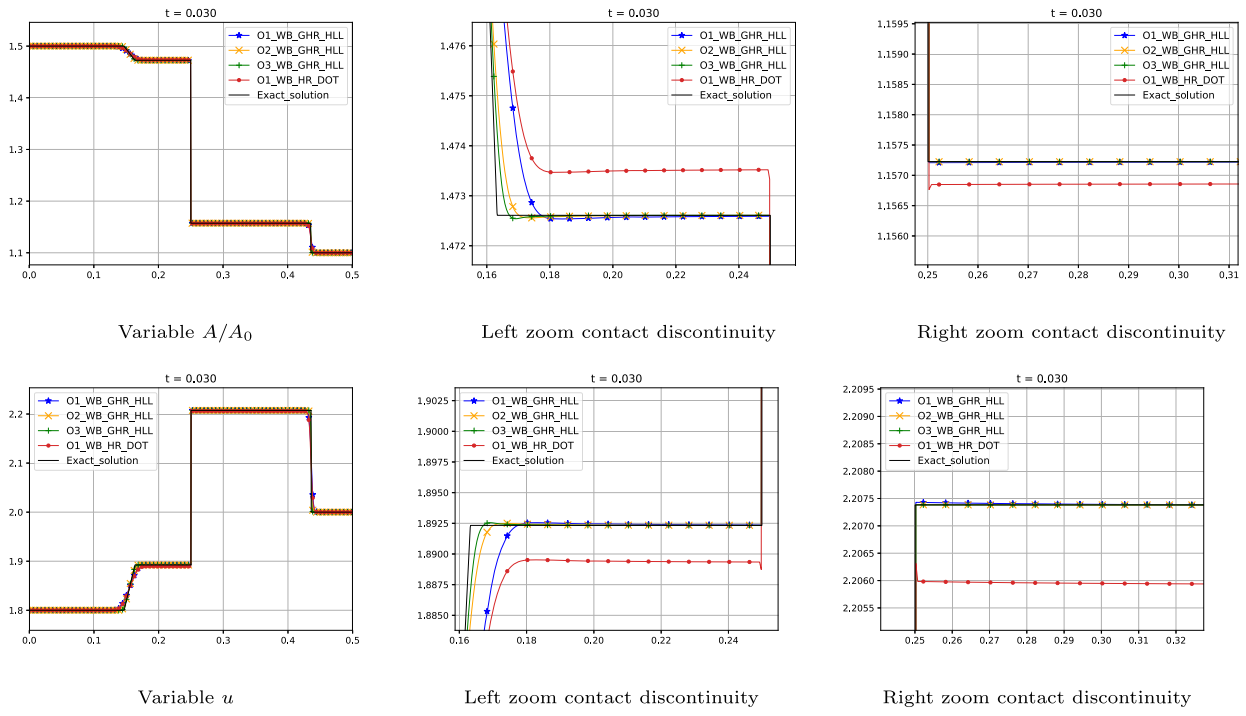

Fig. 4.3.9. Test 15: comparison of the numerical and the exact solutions. Top: variable A/A_0 (left), left zoom contact discontinuity (center), right zoom contact discontinuity (right). Bottom: variable u (left), left zoom contact discontinuity (center), right zoom contact discontinuity (right).

Test 18 This test consists on a subcritical flow composed by a left moving rarefaction followed by a contact discontinuity and a right moving shock. Fig. 4.5.1 shows the numerical results of the fully well-balanced schemes obtained using a mesh of 1000 points. The reference solution has been computed with the first-order fully well-balanced using a fine mesh of 10000 points. We observe that the three of them give accurate results and are able to conserve the total energy Γ (given in (2.20)) across the contact discontinuity as expected.

Test 19 In this test we analyze the behavior of the numerical schemes in the case where we reach the critical blockage condition and the minimum throat section. The flow generated by the left rarefaction reaches a critical vessel area in the narrowest section and a sonic blockage appears. See [49] for details. Fig. 4.5.2 shows the numerical results of the fully well-balanced schemes obtained using a mesh of 1000 points. The reference solution has been computed with the first-order fully well-balanced using a fine mesh of 10000 points. We observe the dissipation of the total energy Γ (given in (2.20)) due to the critical blockage. The three methods seem to capture well the critical blockage condition. We also observe an improvement in the position of the right moving shock when we increase the order of the methods.

5. Conclusions

In this paper, the one-dimensional model for blood flow in thin-walled deformable elastic tubes introduced in [62] is considered. In the context of hyperbolic systems of balance laws, it is well-known that well-balanced methods are necessary to correctly capture the propagation of waves generated by small perturbations of a steady state. Moreover, in [43] the conclusion was reached that fully well-balanced methods, i.e. methods that preserve all the stationary solutions, are necessary as well to correctly capture the steady waves that stand on a discontinuity of one of the mechanical parameters of the blood flow model: the stiffness coefficient. The remaining geometrical and mechanical parameters were assumed to be constant in that reference. The main contribution of this work is to develop high-order fully well-balanced numerical methods for the general case, in which all the parameters may be space varying.

The strategy described in [18] is followed here to develop high-order well-balanced numerical methods. These methods are based on the design of high-order well-balanced reconstruction operators. In order to introduce the numerical methods, first the system is written in a compact form and its nondimensionalization is given. Then, the properties of all its possible stationary solutions are studied. This study is necessary to develop first-, second- and third-order well-balanced reconstruction operators.

Several numerical tests are considered to test the well-balanced properties of the methods and to check that the desired order of accuracy is obtained. The methods are compared with the first-order scheme based on the DOT strategy and the

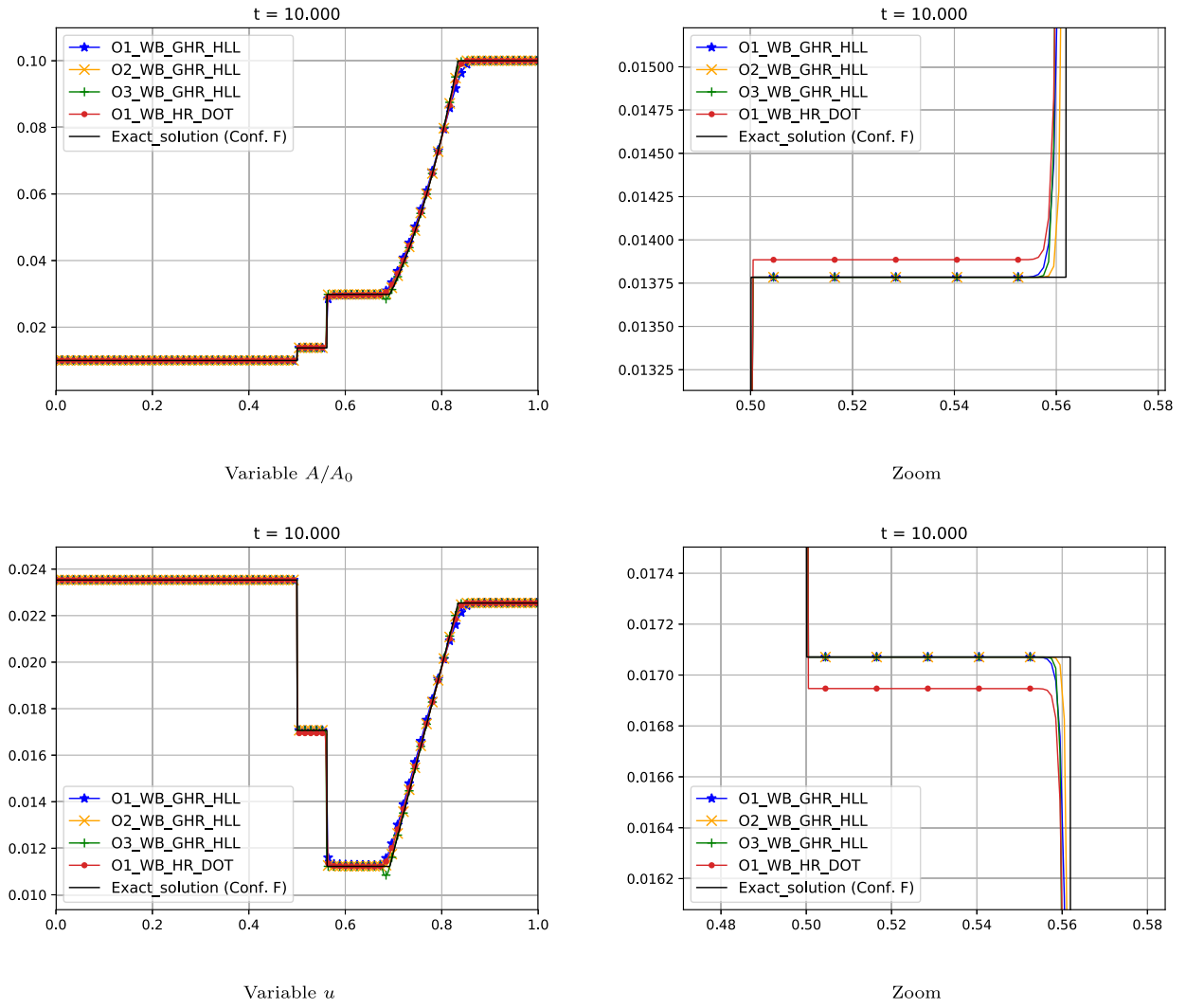

Fig. 4.3.10. Test 16: comparison of the numerical and the exact solution (configuration "F"). Top: variable A/A_0 (left) and zoom (right). Bottom: variable u (left) and zoom (right).

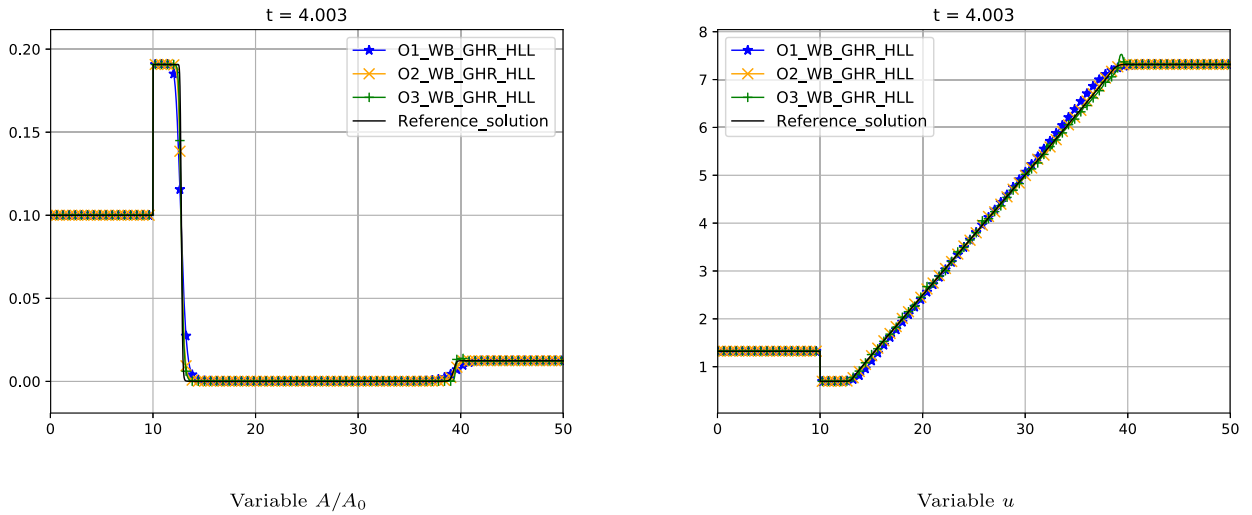

Fig. 4.4.1. Test 17: comparison of the numerical and reference solutions: variables A/A_0 (left) and u (right).

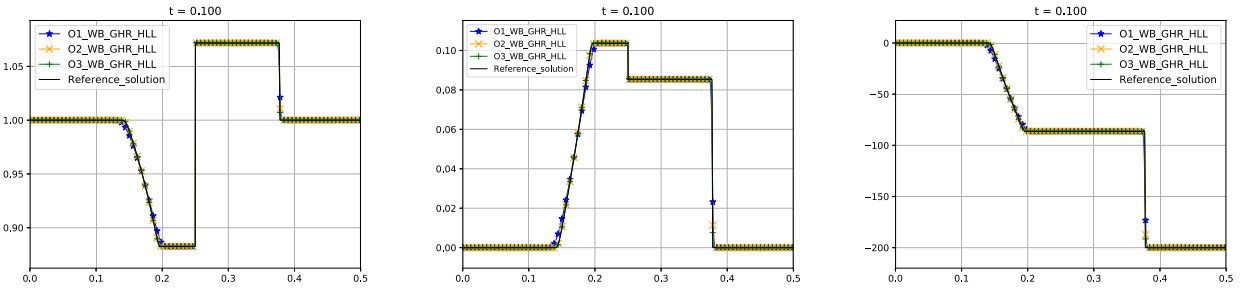

Fig. 4.5.1. Test 18: comparison of the numerical and reference solutions: variables A/A_0 (left), u (center) and total energy: Γ (right).

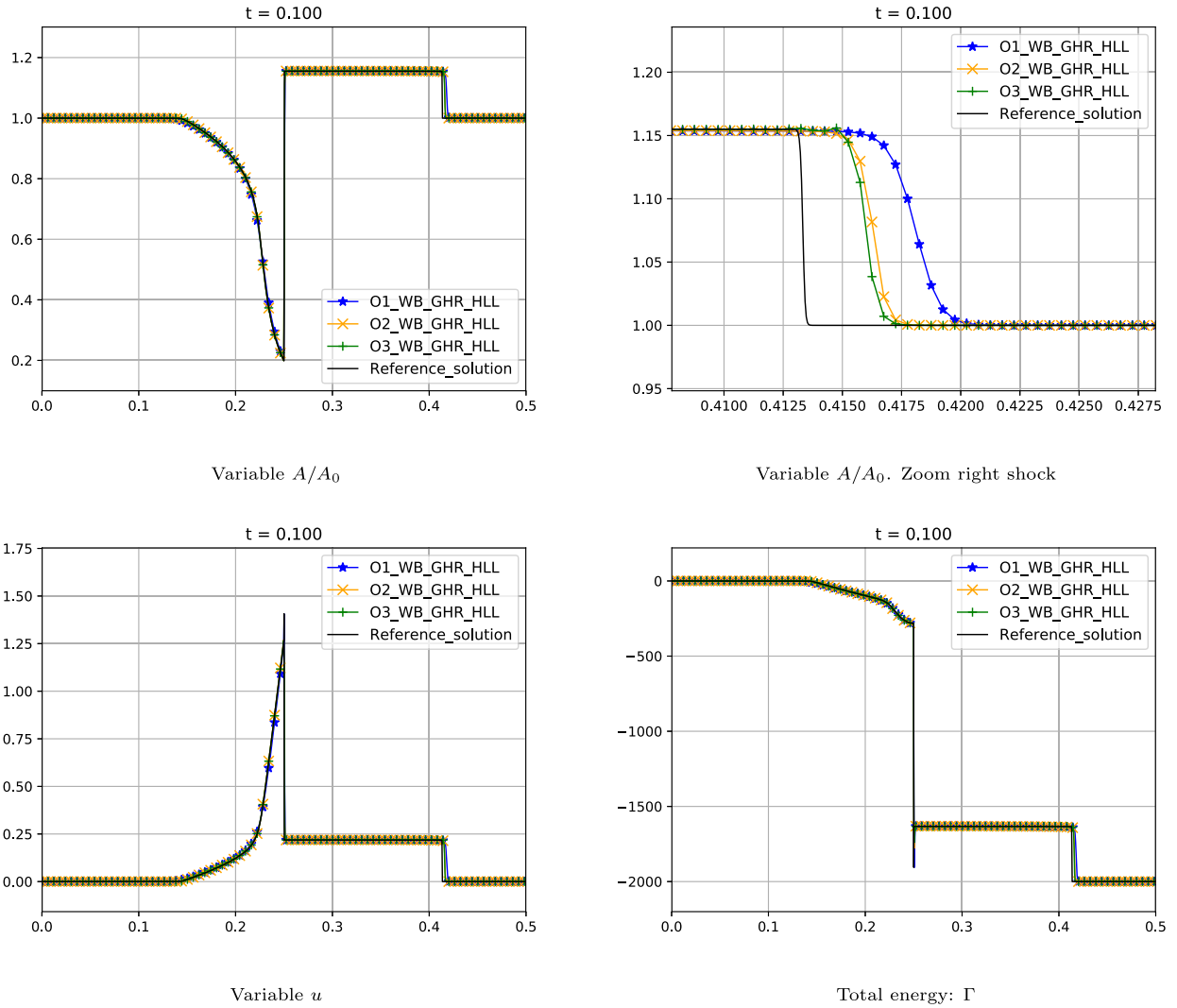

Fig. 4.5.2. Test 19: comparison of the numerical and reference solutions. Top: variable A/A_0 (left) and zoom (right). Bottom: variable u (left) and total energy: Γ (right).

hydrostatic reconstruction technique introduced in [58]. From this exhaustive study the conclusion already reached in [43] about the need of well-balanced methods is confirmed in the general case.

Our future goals are several. On the one hand we want to be able to add the friction term that comes from the viscous resistance of the tube in consideration as in [28,23]. On the other hand, we want to consider the viscoelastic wall effects as in [5]. In these cases the implicit form of stationary solutions is not available so that they have to be numerically approached, as it is done in the well-balanced methods introduced in [29]. Finally we want to use these methods to deal with networks what implies the study of junctions: see [54,41,48].

CRediT authorship contribution statement

Ernesto Pimentel-García: Conceptualization, Formal analysis, Investigation, Methodology, Resources, Software, Validation, Visualization, Writing – original draft, Writing – review & editing. **Lucas O. Müller:** Conceptualization, Formal analysis, Funding acquisition, Investigation, Methodology, Project administration, Resources, Software, Supervision, Validation, Visualization, Writing – review & editing. **Eleuterio F. Toro:** Conceptualization, Formal analysis, Funding acquisition, Investigation, Methodology, Resources, Supervision, Writing – review & editing. **Carlos Parés:** Conceptualization, Formal analysis, Funding acquisition, Investigation, Methodology, Resources, Software, Supervision, Validation, Visualization, Writing – original draft, Writing – review & editing.

Declaration of competing interest

The authors declare the following financial interests/personal relationships which may be considered as potential competing interests: Ernesto and Carlos reports financial support was provided by Spanish Government. Ernesto and Carlos reports financial support was provided by European Regional Development Fund. Ernesto and Carlos reports financial support was provided by Regional Government of Andalusia. Ernesto and Carlos reports financial support was provided by University of Malaga.

Data availability

No data was used for the research described in the article.

Acknowledgements

The research of EPG and CP was partially supported by the Spanish Government (SG), the European Regional Development Fund (ERDF), the Regional Government of Andalusia (RGA), and the University of Málaga (UMA) through the projects of reference RTI2018-096064-B-C21 (SG-ERDF), UMA18-Federja-161 (RGA-ERDF-UMA), and P18-RT-3163 (RGA-ERDF). EPG was also financed by the European Union – NextGenerationEU.

References

[1] R. Abgrall, S. Karni, A comment on the computation of non-conservative products, J. Comput. Phys. 229 (2010) 2759–2763.
[2] E. Audusse, F. Bouchut, M.-O. Bristeau, R. Klein, B. Perthame, A fast and stable well-balanced scheme with hydrostatic reconstruction for shallow water flows, SIAM J. Sci. Comput. 25 (6) (2004) 2050–2065.
[3] A.P. Avolio, Multi-branched model of the human arterial system, Med. Biol. Eng. Comput. 18 (1980) 709–718.
[4] R. Bernetti, V.A. Titarev, E.F. Toro, Exact solution of the Riemann problem for shallow water equations with discontinuous bottom geometry, J. Comput. Phys. 227 (2008) 3212–3243.
[5] G. Bertaglia, V. Caleffi, A. Valiani, Modeling blood flow in viscoelastic vessels: the 1d augmented fluid–structure interaction system, Comput. Methods Appl. Mech. Eng. 360 (2020) 112772.
[6] C. Berthon, A. Duran, F. Foucher, K. Saleh, J.D.D. Zabsonré, Improvement of the hydrostatic reconstruction scheme to get fully discrete entropy inequalities, J. Sci. Comput. 80 (2) (2019) 924–956.
[7] P. Blanco, R. Feijóo, A dimensionally-heterogeneous closed-loop model for the cardiovascular system and its applications, Med. Eng. Phys. 35 (5) (May 2013) 652–667.
[8] P.J. Blanco, G.D. Ares, S.A. Urquiza, R.A. Feijóo, On the effect of preload and pre-stretch on hemodynamic simulations: an integrative approach, Biomech. Model. Mechanobiol. 15 (3) (June 2016) 593–627.
[9] P.J. Blanco, S.M. Watanabe, M.A.R.F. Passos, P.A. Lemos, R.A. Feijoo, An anatomically detailed arterial network model for one-dimensional computational hemodynamics, IEEE Trans. Biomed. Eng. 62 (2) (Feb. 2015) 736–753.
[10] R. Borsche, Numerical schemes for networks of hyperbolic conservation laws, Appl. Numer. Math. 108 (Oct. 2016) 157–170.
[11] F. Bouchut, Nonlinear Stability of Finite Volume Methods for Hyperbolic Conservation Laws: And Well-Balanced Schemes for Sources, Springer Science & Business Media, 2004.
[12] A. Bressan, S. Čanić, M. Garavello, M. Herty, B. Piccoli, Flows on networks: recent results and perspectives, EMS Surv. Math. Sci. 1 (1) (2014) 47–111.
[13] J. Britton, Y. Xing, Well-balanced discontinuous Galerkin methods for the one-dimensional blood flow through arteries model with man-at-eternal-rest and living-man equilibria, Comput. Fluids 203 (May 2020) 104493.
[14] M.J. Castro, J.M. Gallardo, J.A. López-García, C. Parés, Well-balanced high order extensions of Godunov's method for semilinear balance laws, SIAM J. Numer. Anal. 46 (2) (2008) 1012–1039.
[15] M.J. Castro, P.G. LeFloch, M.L. Muñoz-Ruiz, C. Parés, Why many theories of shock waves are necessary: convergence error in formally path-consistent schemes, J. Comput. Phys. 227 (2008) 8107–8129.

[16] M.J. Castro, A. Pardo Milanés, C. Parés, Well-balanced numerical schemes based on a generalized hydrostatic reconstruction technique, Math. Models Methods Appl. Sci. 17 (12) (2007) 2055–2113.
[17] M.J. Castro, C. Parés, Well-balanced high-order finite volume methods for systems of balance laws, J. Sci. Comput. 82 (2) (2020) 1–48.
[18] M.J. Castro, C. Parés, Well-balanced high-order finite volume methods for systems of balance laws, J. Sci. Comput. 82 (2020) 42.
[19] I. Cravero, G. Puppo, M. Semplice, G. Visconti, CWENO: uniformly accurate reconstructions for balance laws, Math. Comput. 87 (312) (2018) 1689–1719.
[20] I. Cravero, M. Semplice, On the accuracy of WENO and CWENO reconstructions of third order on nonuniform meshes, J. Sci. Comput. 67 (3) (2016) 1219–1246.
[21] C.M. Dafermos, The entropy rate admissibility criterion for solutions of hyperbolic conservation laws, J. Differ. Equ. 14 (2) (1973) 202–212.
[22] G. Dal Maso, P.G. LeFloch, F. Murat, Definition and weak stability of nonconservative products, J. Math. Pures Appl. 74 (6) (1995) 483–548.
[23] O. Delestre, P.-Y. Lagrée, A 'well-balanced' finite volume scheme for blood flow simulation, Int. J. Numer. Methods Fluids 72 (2) (2013) 177–205.
[24] M. Dumbser, E.F. Toro, A simple extension of the Osher Riemann solver to non-conservative hyperbolic systems, J. Sci. Comput. 48 (1) (2011) 70–88.
[25] E.T.E. Han, G. Warnecke, A. Siviglia, On Riemann solutions to weakly hyperbolic systems: Part 2. Modelling supercritical flows in arteries, Technical Report NI15004NPA, Isaac Newton Institute for Mathematical Sciences, 2015.
[26] L. Formaggia, D. Lamponi, A. Quarteroni, One-dimensional models for blood flow in arteries, J. Eng. Math. 47 (2003) 251–276.
[27] A. Ghigo, O. Delestre, J.-M. Fullana, P.-Y. Lagrée, Low-Shapiro hydrostatic reconstruction technique for blood flow simulation in large arteries with varying geometrical and mechanical properties, J. Comput. Phys. 331 (Feb. 2017) 108–136.
[28] B. Ghitti, C. Berthon, M.H. Le, E.F. Toro, A fully well-balanced scheme for the 1D blood flow equations with friction source term, J. Comput. Phys. 421 (2020) 109750.
[29] I. Gómez-Bueno, M.J. Castro, C. Parés, High-order well-balanced methods for systems of balance laws: a control-based approach, Appl. Math. Comput. 394 (2021) 125820.
[30] S. Gottlieb, C.-W. Shu, Total variation diminishing Runge-Kutta schemes, Math. Comput. 67 (221) (1998) 73–85.
[31] E.E. Han, M. Hantke, G. Warnecke, Exact Riemann solutions to compressible Euler equations in ducts with discontinuous cross-section, J. Hyperbolic Differ. Equ. 9 (3) (2012) 403–449.
[32] A. Harten, B. Engquist, S. Osher, S.R. Chakravarthy, Uniformly high order accurate essentially non-oscillatory schemes, III, in: Upwind and High-Resolution Schemes, Springer, 1987, pp. 218–290.
[33] A. Harten, P.D. Lax, B. Van Leer, On upstream differencing and Godunov-type schemes for hyperbolic conservation laws, SIAM Rev. 25 (1) (1983) 35–61.
[34] T.J. Hughes, J. Lubliner, On the one-dimensional theory of blood flow in the large vessels, Math. Biosci. 18 (1973) 161–170.
[35] G.-S. Jiang, C.-W. Shu, Efficient implementation of weighted ENO schemes, J. Comput. Phys. 126 (1) (1996) 202–228.
[36] D. Levy, G. Puppo, G. Russo, Central WENO schemes for hyperbolic systems of conservation laws, ESAIM: Math. Model. Numer. Anal. 33 (3) (1999) 547–571.
[37] G. Li, O. Delestre, L. Yuan, Well-balanced discontinuous Galerkin method and finite volume WENO scheme based on hydrostatic reconstruction for blood flow model in arteries., Int. J. Numer. Methods Fluids 86 (7) (Mar. 2018) 491–508.
[38] F. Liang, K. Fukasaku, H. Liu, S. Takagi, A computational model study of the influence of the anatomy of the circle of Willis on cerebral hyperperfusion following carotid artery surgery, Biomed. Eng. Online 10 (1) (2011) 84.
[39] F.Y. Liang, S. Takagi, R. Himeno, H. Liu, Multi-scale modeling of the human cardiovascular system with applications to aortic valvular and arterial stenoses, Med. Biol. Eng. Comput. 47 (2009) 743–755.
[40] X.-D. Liu, S. Osher, T. Chan, Weighted essentially non-oscillatory schemes, J. Comput. Phys. 115 (1) (1994) 200–212.
[41] L.O. Müller, P.J. Blanco, A high order approximation of hyperbolic conservation laws in networks: application to one-dimensional blood flow, J. Comput. Phys. 300 (2015) 423–437.
[42] L.O. Müller, G. Leugering, P.J. Blanco, Consistent treatment of viscoelastic effects at junctions in one-dimensional blood flow models, J. Comput. Phys. 314 (June 2016) 167–193.
[43] L.O. Müller, C. Parés, E.F. Toro, Well-balanced high-order numerical schemes for one-dimensional blood flow in vessels with varying mechanical properties, J. Comput. Phys. 242 (2013) 53–85.
[44] L.O. Müller, E.F. Toro, Well-balanced high-order solver for blood flow in networks of vessels with variable properties, Int. J. Numer. Methods Biomed. Eng. 29 (12) (Dec. 2013) 1388–1411.
[45] L.O. Müller, E.F. Toro, A global multiscale mathematical model for the human circulation with emphasis on the venous system, Int. J. Numer. Methods Biomed. Eng. 30 (7) (July 2014) 681–725.
[46] L.O. Müller, E.F. Toro, M.E. Haacke, D. Utriainen, Impact of CCSVI on cerebral haemodynamics: a mathematical study using MRI angiographic and flow data, Phlebology 31 (5) (June 2016) 305–324.
[47] J. Murillo, P. García-Navarro, A Roe type energy balanced solver for 1d arterial blood flow and transport, Comput. Fluids 117 (2015) 149–167.
[48] J. Murillo, P. García-Navarro, A solution of the junction Riemann problem for 1d hyperbolic balance laws in networks including supersonic flow conditions on elastic collapsible tubes, Symmetry 13 (9) (2021) 1658.
[49] J. Murillo, A. Navas-Montilla, P. García-Navarro, Formulation of exactly balanced solvers for blood flow in elastic vessels and their application to collapsed states, Comput. Fluids 186 (2019) 74–98.
[50] J.P. Mynard, J.J. Smolich, One-dimensional haemodynamic modeling and wave dynamics in the entire adult circulation, Ann. Biomed. Eng. 43 (6) (June 2015) 1443–1460.
[51] M.F. O'Rourke, A.P. Avolio, Pulsatile flow and pressure in human systemic arteries: studies in man and in a multibranched model of the human systemic arterial tree, Circ. Res. 46 (1980) 363–372.
[52] C. Parés, Numerical methods for nonconservative hyperbolic systems: a theoretical framework, SIAM J. Numer. Anal. 44 (1) (2006) 300–321.
[53] K.H. Parker, C.J.H. Jones, Forward and backward running waves in the arteries: analysis using the method of characteristics, J. Biomech. Eng. 112 (1990) 322–326.
[54] F. Piccioli, G. Bertaglia, A. Valiani, V. Caleffi, Modeling blood flow in networks of viscoelastic vessels with the 1-d augmented fluid–structure interaction system, J. Comput. Phys. (2022) 111364.
[55] A. Quarteroni, A. Manzoni, C. Vergara, The cardiovascular system: mathematical modelling, numerical algorithms and clinical applications, Acta Numer. 26 (May 2017) 365–590.
[56] W. Sheng, Q. Zhang, Y. Zheng, The Riemann problem for a blood flow model in arteries, Commun. Comput. Phys. 27 (2020) 227–250.
[57] Y. Shi, P. Lawford, R. Hose, Review of zero-d and 1-d models of blood flow in the cardiovascular system, Biomed. Eng. Online 10 (1) (2011) 33.
[58] A. Spilimbergo, E.F. Toro, L.O. Müller, One-dimensional blood flow with discontinuous properties and transport: mathematical analysis and numerical schemes, Commun. Comput. Phys. 29 (3) (2021) 649–697.
[59] B.N. Steele, Using one-dimensional finite element analysis to estimate differential pressure of renal artery stenoses, Comput. Cardiol. 34 (2007) 391–394.
[60] E.F. Toro, M. Celant, Q. Zhang, C. Contarino, N. Agarwal, A. Linninger, L.O. Müller, Cerebrospinal fluid dynamics coupled to the global circulation in holistic setting: mathematical models, numerical methods and applications, Int. J. Numer. Methods Biomed. Eng. 38 (1) (Jan. 2022).
[61] E.F. Toro, L.O. Müller, A. Siviglia, Bounds for wave speeds in the Riemann problem: direct theoretical estimates, Comput. Fluids 209 (2020) 104640.

[62] E.F. Toro, A. Siviglia, Flow in collapsible tubes with discontinuous mechanical properties: mathematical model and exact solutions, Commun. Comput. Phys. 13 (2) (2013) 361–385.
[63] B. Van Leer, Towards the ultimate conservative difference scheme. II. Monotonicity and conservation combined in a second-order scheme, J. Comput. Phys. 14 (4) (1974) 361–370.